

How does a dark compact object ringdown?

Elisa Maggio,^{1,*} Luca Buoninfante,^{2,†} Anupam Mazumdar,^{3,‡} and Paolo Pani^{1,§}

¹*Dipartimento di Fisica, “Sapienza” Università di Roma & Sezione INFN Roma1, Roma 00185, Italy*

²*Department of Physics, Tokyo Institute of Technology, Tokyo 152-8551, Japan*

³*Van Swinderen Institute, University of Groningen, 9747 AG, Groningen, The Netherlands*

A generic feature of nearly out-of-equilibrium dissipative systems is that they resonate through a set of quasinormal modes. Black holes – the absorbing objects *par excellence* – are no exception. When formed in a merger, black holes vibrate in a process called “ringdown”, which leaves the gravitational-wave footprint of the event horizon. In some models of quantum gravity which attempt to solve the information-loss paradox and the singularities of General Relativity, black holes are replaced by regular, horizonless objects with a tiny effective reflectivity. Motivated by these scenarios, here we develop a generic framework to the study of the ringdown of a compact object with various shades of darkness. By extending the black-hole membrane paradigm, we map the interior of any compact object in terms of the bulk and shear viscosities of a fictitious fluid located at the surface, with the black-hole limit being a single point in a three-dimensional parameter space. We unveil some remarkable features of the ringdown and some universal properties of the light ring in this framework. We also identify the region of the parameter space which can be probed by current and future gravitational-wave detectors. A general feature is the appearance of mode doublets which are degenerate only in the black-hole limit. We argue that the merger event GW150914 already imposes a strong lower bound on the compactness of the merger remnant of approximately 99% of the black-hole compactness. This places model-independent constraints on black-hole alternatives such as diffuse “fuzzballs” and nonlocal stars.

I. INTRODUCTION

At the beginning of the last century, the quantum description of atomic interactions had been dramatically revolutionized by *precision* atomic spectroscopy. The observation of a small effect such as the Lamb shift in the energy levels of the hydrogen atom [1] had a paramount impact in shaping the development of quantum electrodynamics. Following the historical detection of the gravitational waves (GWs) from binary mergers [2, 3], black-hole (BH) spectroscopy [4–10] – i.e., the measurement of the GW spectrum of a BH through post-merger “ringdown” observations [2, 11] – may play a similar major role in probing the gravitational interaction and fundamental physics [12–15].

Indeed, BHs can be considered as the “hydrogen atom” of gravity, and their GW spectrum is their characteristic footprint. At variance with the hydrogen atom, though, BHs are *dissipative* systems and their spectrum is described by quasinormal modes (QNMs), each one defined by an oscillation frequency ω and a damping time τ related to the dissipation due to the GW emission at infinity and the absorption at the horizon.

The defining feature of a BH is its event horizon, i.e., a hypersurface delimiting the spacetime region from which no signal can escape. Accordingly, BHs are perfect absorbers at the classical level¹. The presence of a horizon

provides the key to reading BH physics [17]: the strong redshift near these objects, the existence of a photon-sphere [18, 19], the number of independent “charges”, their multipole moments, their vanishing tidal deformability, and last but not least their QNM spectrum.

Nonetheless, the presence of an event horizon poses some theoretical and fundamental problems [17], the most notable ones being the presence of a curvature singularity inside BHs (where Einstein’s theory breaks down) and the Hawking information loss paradox (according to which unitarity of quantum mechanics is lost if a spacetime has an event horizon [20]). Different attempts to solve these long-standing problems have been proposed. Many of them share the common feature that classical BHs are replaced by horizonless, singularity-free solutions. This is the case of the “fuzzball” proposal [21–23], according to which a large number of regular, horizonless microstate geometries with the same asymptotic charges of a BH emerge as solutions to supergravity and string theories [23–27]. Another example are nonlocal stars [28] that emerge in theories with infinite-derivatives in which the nonlocality of the gravitational interaction can smear out the curvature singularity and avoid the presence of a horizon [29–34].

In this context, the devising of observational tests to distinguish a classical BH from another dark compact object is of utmost importance, and current GW observations (such as GW190814 [35]) do not exclude the existence of exotic compact objects other than BHs and neutron stars. Arguably, GW spectroscopy is the most

* elisa.maggio@uniroma1.it

† buoninfante.l.aa@m.titech.ac.jp

‡ anupam.mazumdar@rug.nl

§ paolo.pani@uniroma1.it

¹ For astrophysical BHs, the semi-classical phenomenon of Hawking radiation [16] is negligible.

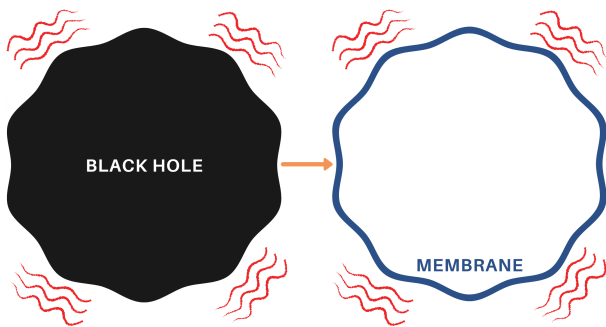


FIG. 1. Schematic representation of the BH membrane paradigm [36, 37]. A static observer outside the horizon can replace the interior of a perturbed BH (left) with a perturbed fictitious membrane (right). The membrane is made of a viscous fluid whose properties (density, pressure, viscosity) are fixed to reproduce the BH phenomenology, in particular the QNM spectrum. In this paper we extend this concept to a generic dark compact object, parametrizing its properties in terms of the membrane’s physical quantities.

direct way to test the nature of a remnant formed in the highly-dynamical aftermath of a gravitational merger. Even small deviations in the QNMs predicted for a BH in General Relativity might provide indication for new physics, similarly to the Lamb shift in the spectrum of the hydrogen atom.

A dark compact object can be identified by two parameters, quantifying its shades of “darkness” and its “compactness” [17]. The darkness of the object depends on its reflectivity, whereas the compactness is related to the gravitational redshift at its surface. It has been shown that the prompt ringdown signal which follows the merger is universal if the remnant is sufficiently compact [38–40]. Putative near-horizon structures, which can be modelled in terms of a reflectivity coefficient at the surface of the object [41, 42], show up only at late times in the form of repeated and modulated “GW echoes” [38–40, 43]. The time delay between echoes depends on the compactness of the object, whereas the relative amplitude between subsequent echoes is related to the reflectivity. Considerable attention has been devoted to the study of this signal in a variety of models of near-horizon quantum structures [44–49], in the context of exotic compact objects in General Relativity [50, 51], and for modified-gravity scenarios [28, 52–54]. Phenomenological waveform models have also been analyzed in detail [41, 55–62] and implemented in actual searches in LIGO/Virgo data [43, 44, 60, 63–68] (see Refs. [17, 69] for some reviews).

The above studies focused on the case of objects almost as compact as a BH, but with some nonvanishing reflectivity. However, in what can be arguably considered as the best-motivated attempts to solve the information-loss paradox, the reflectivity is expected to be very small, for example owing to the enormous number of degrees of freedom that can be excited within a fuzzball [70] or due to

nonlocal effects [28]. These solutions can be less compact than BHs; therefore, they could emit a ringdown signal which differs from the BH ringdown at early stages.

In this paper, we propose a generic and (as much as possible) model-independent framework to study the ringdown of a dark compact object in the context of General Relativity or some of its high-energy extensions. We unveil some universal features of the ringdown and show that current GW observations can already place very stringent constraints on the compactness of a dark object.

II. MEMBRANE PARADIGM FOR PERTURBED COMPACT OBJECTS

A. Setup

Our framework extends the seminal work by Damour, MacDonald, Price, Thorne, Znajek, and others on the BH membrane paradigm [36, 37, 71]. In its standard formulation (see Fig. 1), a static observer can replace the BH interior with a *fictitious* membrane located at the horizon. The features of the internal spacetime are projected onto the membrane, whose physical properties are fixed by the Israel-Darmois junction conditions [72–74] (we assume $G = c = 1$ units throughout),

$$[[h_{ab}]] = 0, \quad [[K_{ab} - h_{ab}K]] = -8\pi T_{ab}, \quad (1)$$

where h_{ab} is the induced metric on the membrane, K_{ab} is the extrinsic curvature, $K = K_{ab}h^{ab}$, T_{ab} is the stress-energy tensor of the matter distribution located on the membrane, and $[[...]]$ denotes the jump of a quantity across the membrane. The junction conditions impose that the fictitious membrane is described by a viscous fluid whose thermodynamical properties (density, pressure, viscosity parameters) are uniquely determined if the membrane is demanded to act as a BH in terms of observable effects [37, 75]. We work in the framework of General Relativity² and, for simplicity, we assume spherical symmetry.

B. Background geometry

Let us assume that the fictitious membrane is located at the surface of the compact object, $r = R$, in

² Although our framework can be applied to any theory of gravity, in practice, we assume that General Relativity works sufficiently well near the radius of the compact object. This assumption is well justified also for solutions to modified gravity in which putative extra degrees of freedom are heavy. In this case, all corrections to the metric and field equations are suppressed by powers of $\ell_P/R \ll 1$, where R is the object radius, and ℓ_P is the Planck length or the scale of new physics. For compact astrophysical objects, such corrections are negligible. No specific theory is assumed to describe the object interior.

some coordinate system. Owing to Birkhoff's theorem, the spacetime geometry for $r > R$ is described by the Schwarzschild metric,

$$ds^2 = -f(r)dt^2 + \frac{1}{f(r)}dr^2 + r^2(d\theta^2 + \sin^2\theta d\varphi^2), \quad (2)$$

where $f(r) = 1 - 2M/r$ and M is the total mass of the object. It is convenient to parametrize the circumferential radius of the membrane as

$$R = 2M(1 + \epsilon), \quad (3)$$

which defines the compactness of the object, M/R . When $\epsilon \rightarrow 0$ the membrane location coincides with the Schwarzschild's horizon, $R = 2M$, whereas when $\epsilon = 1/2$ it coincides with the light ring (or photon-sphere), $R = 3M$, where circular, unstable photon orbits reside. As we shall show, in the latter limit some remarkable and universal properties of the QNM spectrum emerge. The case of $\epsilon \ll 1$ corresponds to ultracompact configurations characterized, for instance, by microscopic corrections at the horizon scale, whereas the case of $\epsilon \sim \mathcal{O}(0.1 - 1)$ corresponds to less compact objects whose compactness is comparable to or larger than that of a neutron star. In the context of fuzzballs, the former and latter cases describe tight and diffuse fuzzball models [70], respectively. The model of nonlocal stars introduced in [28] is characterized by a maximal compactness of the order of the Buchdahl limit [76], i.e., $\epsilon \simeq 0.125$, and therefore belongs to the latter category.

Following the original membrane paradigm, we assume that the fictitious membrane is such that the extrinsic curvature of the internal spacetime vanishes, $K_{ab}^- = 0$ [37]. The details of the computation are given in Appendix A, here we only summarize the main results. The junction conditions are compatible with a membrane described by the stress-energy tensor of a dissipative fluid [37, 77]:

$$T_{ab} = \rho u_a u_b + (p - \zeta\Theta)\gamma_{ab} - 2\eta\sigma_{ab}, \quad (4)$$

where ρ , p , and u_a are the density, the pressure, and the 3-velocity of the fluid, respectively, whereas Θ is the expansion, σ_{ab} is the shear tensor, and $\gamma_{ab} = h_{ab} + u_a u_b$ is the projector tensor. The parameters ζ and η are the bulk and the shear viscosities that govern the response of the fluid to external perturbations. For a given model of the interior of the compact object, η and ζ are uniquely determined. In general, they depend on the density (and the temperature) of the fluid and can be frequency-dependent, complex numbers. Since energy dissipation is absent when $\Re[\eta] = 0 = \Re[\zeta]$, for simplicity in the following we shall consider η and ζ to be real constants, although our framework can be straightforwardly generalized.

When the object is unperturbed, the viscosity is irrelevant and the spherical membrane is described by a perfect fluid. The junction conditions then give the pressure and

density of the fluid

$$p(R) = \frac{2f(R) + Rf'(R)}{16\pi R\sqrt{f(R)}}, \quad \rho(R) = -\frac{\sqrt{f(R)}}{4\pi R}, \quad (5)$$

which parametrically fix a barotropic equation of state, $p = p(\rho)$. In the BH limit, the density vanishes and the pressure diverges as the redshift factor $\epsilon^{-1/2}$. The speed of sound, $c_s = \sqrt{\partial p / \partial \rho}$, diverges both in the BH limit ($\epsilon \rightarrow 0$) and in the light-ring limit ($\epsilon \rightarrow 1/2$). However, it is important to stress that these pathologies of the fluid are not an issue since the membrane is fictitious.

C. Linear perturbations & boundary conditions

Gravitational perturbations in the exterior Schwarzschild geometry are governed by two simple equations that can be both written in a Schrödinger-like form [5, 78–80],

$$\frac{d^2\psi(x)}{dx^2} + [\omega^2 - V(r)]\psi(x) = 0, \quad (6)$$

where the effective potential $V(r)$ reads

$$V_{\text{axial}} = f \left(\frac{l(l+1)}{r^2} - \frac{6M}{r^3} \right), \quad (7)$$

$$V_{\text{polar}} = 2f \left(\frac{q^2(q+1)r^3 + 3q^2Mr^2 + 9M^2(qr+M)}{r^3(qr+3M)^2} \right), \quad (8)$$

for axial (i.e., magnetic or odd-parity) and polar (i.e., electric or even-parity) perturbations, respectively. Here x is the ‘‘tortoise’’ coordinate such that $dx/dr = 1/f(r)$, $q = \frac{1}{2}(l-1)(l+2)$, and l is the angular number of the perturbation.

By imposing boundary conditions at infinity and at the inner boundary, Eq. (6) defines an eigenvalue problem whose complex³ eigenvalues are the QNMs of the system, $\omega = \omega_R + i\omega_I$. The effective potential vanishes at infinity, so the general solution to Eq. (6) in the asymptotic region is a superposition of ingoing and outgoing waves. The QNMs are defined by imposing purely outgoing waves at infinity

$$\psi(x) \sim e^{i\omega x}, \quad x \rightarrow \infty. \quad (9)$$

In the BH case, regularity at the horizon (located at $x \rightarrow -\infty$ in tortoise coordinates) implies purely ingoing waves at the inner boundary,

$$\psi_{\text{BH}}(x) \sim e^{-i\omega x}, \quad x \rightarrow -\infty, \quad (10)$$

for both axial and polar perturbations.

³ In our conventions a stable mode corresponds to $\omega_I < 0$, whereas an unstable mode corresponds to $\omega_I > 0$.

In the general case, the condition on the inner boundary depends on the properties of the object, in particular on its compactness and reflectivity. In order to derive these boundary conditions generically (i.e., without assuming any specific solution for the interior of the object), we rely on the membrane paradigm and impose junction conditions on the perturbations at the membrane. As detailed in Appendix A, the generic boundary condition for the axial case turns out to be

$$\frac{\psi'(x)}{\psi(x)} = -\frac{i\omega}{16\pi\eta} - \frac{R^2}{2(R-3M)}V_{\text{axial}}(R), \quad x \rightarrow x_R \quad (11)$$

where the prime denotes the derivative with respect to the tortoise coordinate, and $x_R \equiv x(R)$. The polar case is more involved but a similar computation yields

$$\frac{\psi'(x)}{\psi(x)} = -16\pi i\eta\omega + G(R, \omega, \eta, \zeta), \quad x \rightarrow x_R \quad (12)$$

where G is a complicated function given in Appendix A.

The boundary conditions given by Eq. (11) and Eq. (12) are one of our main results: they are valid for *any* compact object described by a Schwarzschild exterior and have far-reaching consequences, which we discuss in the following.

The linear response of the object in the time domain is governed by the partial differential equation $[\partial_t^2 - \partial_x^2 + V]\hat{\psi}(t, x) = 0$, where $\hat{\psi}(t, x)$ is the inverse Fourier transform of $\psi(\omega, x)$. In the axial sector, the time-domain response can be computed straightforwardly, since the inverse Fourier transform of the boundary condition (11) reads

$$\partial_x \hat{\psi}(t, x_R) = \frac{1}{16\pi\eta} \partial_t \hat{\psi}(t, x_R) - \frac{R^2 V_{\text{axial}}(R)}{2(R-3M)} \hat{\psi}(t, x_R). \quad (13)$$

The polar sector is more involved since the dependence on ω in Eq. (12) is complicated and the inverse Fourier transform cannot be obtained in closed form.

D. Effective viscosity, reflectivity, and universality

In the BH limit the boundary conditions in Eqs. (11) and (12) must reduce to the BH one. A straightforward inspection of the above formulas shows that, when $R \rightarrow 2M$, the BH boundary condition in Eq. (10) is recovered only if

$$\eta = \frac{1}{16\pi} \equiv \eta_{\text{BH}}. \quad (14)$$

In this case Eq. (13) reduces to $\partial_x \psi(t, x) = \partial_t \psi(t, x)$, i.e., the standard boundary condition for an ingoing wave $\sim e^{-i\omega(t+x)}$ near the horizon. Thus, a perturbed BH of mass M behaves as a $(2+1)$ -dimensional viscous fluid located at $r = R \sim 2M$ with shear viscosity $\eta = 1/(16\pi)$. This result agrees with the standard BH membrane paradigm and extends the results of Refs. [69, 77] to the polar sector.

Unlike the axial sector, the polar boundary condition depends explicitly on the bulk viscosity ζ . However, when $R \rightarrow 2M$ the dependence on ζ disappears, so this parameter is not fixed by the linear perturbation analysis in the BH limit (see Appendix A for details). On the other hand, according to the membrane paradigm, a generic BH can be mapped in terms of a fluid also endowed with a *negative* bulk viscosity, $\zeta = -1/(16\pi) \equiv \zeta_{\text{BH}}$. This peculiar property is associated with the *teleological* nature of the event horizon [37].

One might wonder about the physical meaning of the shear viscosity as given in Eq. (14). For this purpose, it is instructive to compute the reflectivity coefficient $|\mathcal{R}|^2$ of the object. The latter is defined through the scattering of a wave coming from infinity with (say) unitary amplitude and being partly reflected back, i.e.

$$\psi(x) \sim \mathcal{R}e^{i\omega x} + e^{-i\omega x}, \quad x \rightarrow \infty, \quad (15)$$

after being subjected to the boundary conditions (11) or (12) at $r = R$.

It is straightforward to compute \mathcal{R} in the large-frequency⁴ limit ($M\omega \gg 1$), where the effective potential in Eq. (6) can be neglected. In this case, we obtain a simple analytical result valid for both axial and polar perturbations:

$$|\mathcal{R}|^2 = \left(\frac{1 - \eta/\eta_{\text{BH}}}{1 + \eta/\eta_{\text{BH}}} \right)^2. \quad (16)$$

This shows that the object is a *perfect absorber* ($|\mathcal{R}|^2 = 0$) of high-frequency waves if and only if $\eta = \eta_{\text{BH}}$, whereas it becomes a *perfect reflector* ($|\mathcal{R}|^2 = 1$) of high-frequency waves when either $\eta = 0$ or $\eta \rightarrow \infty$. In the case of an ultracompact object with $\epsilon \ll 1$ and for any frequency, the former and latter cases correspond to Dirichlet ($\psi = 0$) and Neumann ($\psi' = 0$) boundary conditions, respectively, for the axial sector. As clear from Eq. (12), the opposite is true for the polar sector: $\eta = 0$ ($\eta \rightarrow \infty$) corresponds to the Neumann (Dirichlet) boundary condition. These perfectly reflecting boundary conditions were studied in Refs. [42, 81], of which our results are a generalization.

Although η is formally a free parameter, we expect the most interesting range to be $\eta \in [0, \eta_{\text{BH}}]$. Indeed, from Eq. (16) negative values of η would correspond to $|\mathcal{R}|^2 > 1$, which leads to superradiant instabilities [82] even in the static case. Similarly, for $\eta > \eta_{\text{BH}}$ the reflectivity coefficient is a monotonically growing function of the shear viscosity, which is also unphysical.

The reflectivity coefficient for generic frequencies can be computed numerically with standard methods (see e.g., Ref. [82]). The result is shown in Fig. 2 for axial (left panel) and polar (right panel) perturbations and some

⁴ For an object with $M = 10M_{\odot}$, radio waves with frequency $\gg 3$ kHz are already in the large-frequency regime.

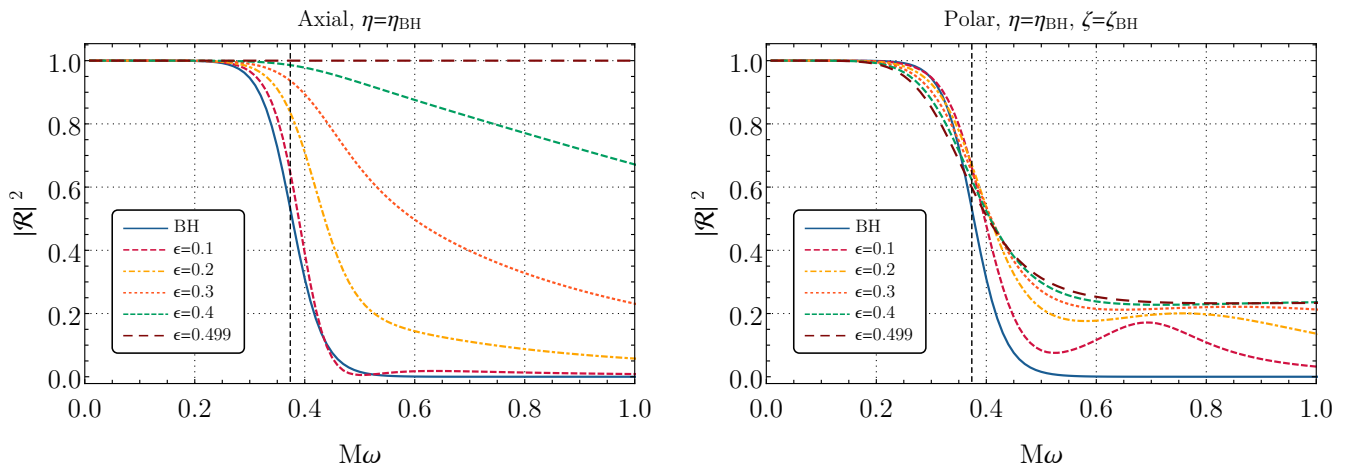


FIG. 2. Reflectivity coefficient of a dark compact object for axial (left panel) and polar (right panel) perturbations in terms of the shear ($\eta = \eta_{\text{BH}}$) and the bulk ($\zeta = \zeta_{\text{BH}}$) viscosities of a fictitious fluid located at the surface of the object, $R = 2M(1 + \epsilon)$, and for several values of ϵ . At high frequency, $M\omega \gg 1$, the object is perfectly absorbing for any value of ϵ [see Eq. (16)]. Interestingly, for $\epsilon \rightarrow 1/2$ the object becomes a perfect reflector of axial GWs for all frequencies and regardless of the values of η (not shown in the plot). In both panels the vertical dashed line corresponds to the fundamental QNM frequency of a Schwarzschild BH, $M\omega_{\text{R}}^{\text{BH}} \approx 0.3737$.

representative choices of the parameters. Besides recovering all the expected limits with respect to the BH case and in the large-frequency regime, this plot also shows some other interesting effects.

Noticeably, as $\epsilon \rightarrow 1/2$ (i.e., as the surface of the object approaches the light ring), the reflectivity coefficient of axial GWs tends to unity for any frequency. This can be understood by looking at the boundary condition (11), whose last term diverges as $R \rightarrow 3M$, thus imposing $\psi = 0$ for any frequency and for any $\eta \in \mathbb{C}$. Therefore, regardless of its internal structure, an object with $R = 3M$ is a *perfect reflector* of axial GWs⁵. The polar sector does not enjoy the same universality. Moreover, in some regions of the parameter space the polar reflectivity shows some distinctive peak at specific frequencies, as shown in Fig. 2 for $\epsilon = 0.1$ (for the choice $\eta = \eta_{\text{BH}}$ and $\zeta = 0$ not shown in the plot the peak can be as high as $|\mathcal{R}|^2 = 1$).

It is also interesting to note that the reflectivity of the spacetime at intermediate frequencies ($M\omega = \mathcal{O}(0.1-1)$), those relevant in the ringdown [11]) can be larger than the BH reflectivity even if the object is a perfect absorber at higher frequencies. For example, at the fundamental BH QNM frequency, $M\omega \approx 0.3737$ (shown in Fig. 2 as a vertical dashed line), the reflectivity is $|\mathcal{R}|^2 \approx 1$ for axial perturbations, $\epsilon = 0.4$ and $\eta = \eta_{\text{BH}}$, although $|\mathcal{R}|^2 \rightarrow 0$ as $M\omega \gg 1$.

⁵ The only exception is when $\eta \rightarrow -\frac{3i\omega}{16\pi q}(R-3M)$ as $R \rightarrow 3M$, in which case the divergence in Eq. (11) cancels out. However, for any purely imaginary η the axial reflectivity is unity at any frequency, so the object remains a perfect reflector. Although very fine-tuned, this particular case corresponds to thin-shell gravastars [83, 84].

These effects have dramatic consequences for the ringdown and the QNM spectrum, as we are going to discuss in the next section.

III. RINGDOWN & QNM SPECTRUM

Equation (6) with boundary conditions (9) and either (11) (for the axial case) or (12) (for the polar case) can be solved numerically as an eigenvalue problem to derive the QNM spectrum of a given model, identified by the parameters (ϵ, η, ζ) . For each value of $l = 2, 3, \dots$, there exists a countably infinite set of QNMs which can be ordered ($n = 0, 1, 2, \dots$) in terms of their imaginary part, $\Im(\omega) \equiv \omega_I$: the fundamental mode ($n = 0$) has the longest decay time, $\tau = -1/\omega_I$, whereas its overtones ($n = 1, 2, \dots$) have a shorter lifetime.

In the axial case the QNM spectrum depends on the two-dimensional parameter space (ϵ, η) – i.e., on the compactness and viscosity of the membrane – whereas in the polar sector there is an additional dependence on the bulk viscosity ζ . As previously discussed, in the $\epsilon \rightarrow 0$ limit the polar boundary conditions (and hence the QNMs) are independent of ζ .

We compute the QNM spectrum using two numerical methods [85]: a shooting method based on the direct integration of Eq. (6), and another one based on continued fractions [10, 86] in a variant adapted from the case of compact stars [87–89]. The continued-fraction method is more robust as it is well suited also for overtones with $M\omega_I \gg 1$, for which the direct integration fails. When both applicable, the two methods are in excellent agreement.

A. Prompt ringdown versus GW echoes

Before proceeding with the QNM analysis, let us look at the linear response in the time domain by studying a wave packet scattered off the object. Since the external spacetime for $r > R$ is described by the Schwarzschild metric, the initial, *prompt ringdown* is associated with the scattering of the wave packet off the effective potential $V(r)$ [see Eq. (6)] independently of the boundary conditions. Indeed, if ϵ is sufficiently small the following causality argument shows that the boundary conditions cannot affect the prompt ringdown [38]. The decay time scale of the prompt ringdown is associated with the instability time scale of circular photon orbits at the light ring [17, 18], or equivalently to the decay time of the fundamental QNM of a Schwarzschild BH, $\tau = -1/\omega_I \approx 10M$. Thus, the boundary conditions at $r = R (< 3M)$ do not have time to modify the prompt ringdown if the round-trip time of the radiation from the photon sphere to the boundary and back [17, 39, 40],

$$\tau_{\text{echo}} = 2M [1 - 2\epsilon - 2 \log(2\epsilon)] , \quad (17)$$

is much longer than $\approx 10M$. This imposes $\epsilon \ll \mathcal{O}(0.01)$ [17]. Objects with such a large compactness were dubbed *ClePhOs*, since they have a clean photon-sphere [17, 40]. On the other hand, if $\epsilon \gtrsim \mathcal{O}(0.01)$ the object's interior is expected to affect the prompt ringdown.

These expectations are confirmed by the ringdown waveforms shown in Fig. 3, which are obtained by solving the linearized problem for axial perturbations with boundary condition (13) using a fourth-order Runge-Kutta finite-difference scheme. The top panel shows the $\epsilon \rightarrow 0$ limit. Confirming previous results [38–40], in this case the prompt ringdown is universal and the details of the object's interior appear only in late-time echoes of the initial ringdown. Their period is roughly given by Eq. (17), and their frequency content and phase are modulated by the boundary conditions and by the tunneling through the potential barrier [61, 62]. Finally, their amplitude depends on the shear viscosity η . In particular, $\eta \approx 0$ corresponds to $|\mathcal{R}|^2 \approx 1$ for which subsequent echoes amplitudes are only mildly damped [61], whereas absorption is maximized as $\eta \rightarrow \eta_{\text{BH}}$. In the latter case the linear response is identical to that of a BH, since the boundary conditions are the same when $\eta \rightarrow \eta_{\text{BH}}$ and $\epsilon \rightarrow 0$.

The bottom panel of Fig. 3 focuses on the case $\epsilon \gtrsim \mathcal{O}(0.01)$, where the prompt ringdown is modified and no subsequent echoes appear. The changes to the prompt ringdown can be understood by considering that the part of the wave packet that initially tunnels through the barrier has enough time to be reflected at $r = R$ and to tunnel again to infinity. This process results in a superposition of the two pulses (the one directly reflected by the potential barrier and the one reflected by the object), which interfere in a complicated pattern. When the two pulses sum in phase, the interference produces

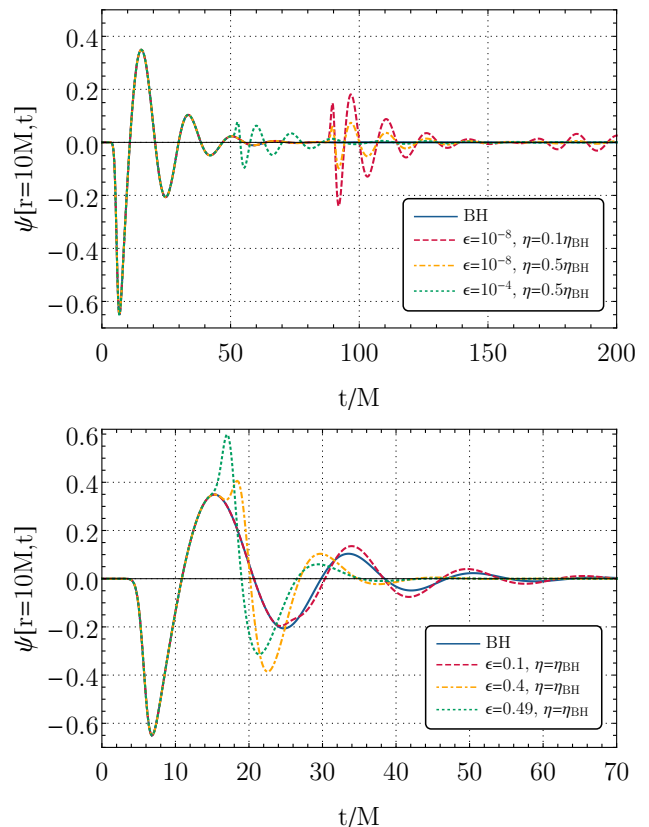


FIG. 3. Ringdown of a dark compact object with radius $R = 2M(1 + \epsilon)$ and effective shear viscosity η . We consider axial perturbations and an initial Gaussian profile, $\psi(x, 0) = 0$, $\partial_t \psi(x, 0) = \exp[-(x - 7)^2]$. Top panel: when $\epsilon \ll 0.01$ GW echoes appear for several values of η related to the reflectivity of the object. Bottom panel: a selection of ringdown waveforms for $\epsilon > 0.01$. In this case echoes are absent but the prompt ringdown is governed by the modified QNMs of the object.

higher peaks in the prompt ringdown. Crucially, as discussed in the following section, at late time the prompt ringdown is dominated by the fundamental QNM of the object, which is *not* the mode of the universal prompt ringdown in the BH case.

Finally, one might wonder why there are no echoes for $\epsilon \gtrsim \mathcal{O}(0.01)$, even though the reflectivity of the object at intermediate frequencies is high, as shown in Fig. 2. The reason is that only waves with frequency $V(R) < \omega^2 < V_{\text{max}}$ can be trapped between the object surface and the potential barrier. Therefore, when the compactness decreases, the resulting cavity is small. Furthermore, the transmission coefficient of the potential barrier is large when $\omega^2 \lesssim V_{\text{max}}$, which implies that these frequencies cannot be trapped efficiently. This also explains why when $R \rightarrow 3M$ (corresponding to perfect reflection of axial GWs) there are no echoes, since the membrane is very close to the maximum of the potential. In practice, for $\epsilon \gtrsim \mathcal{O}(0.01)$ one sees only the interference between the prompt ringdown and the first echo, while subsequent

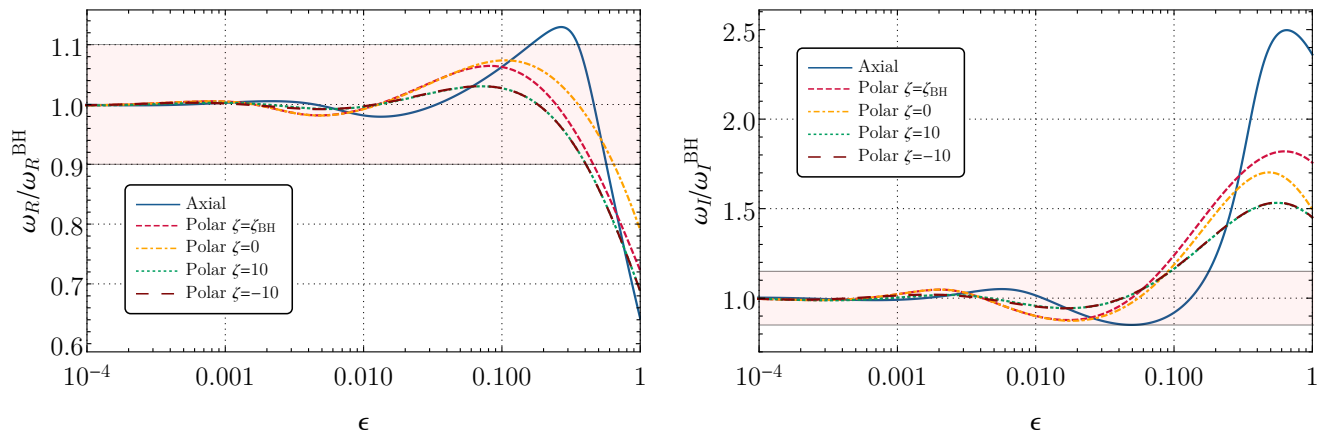


FIG. 4. Real (left panel) and imaginary (right panel) part of the fundamental ($l = 2$) QNM of a dark compact object with effective shear viscosity $\eta = \eta_{\text{BH}}$, with respect to their corresponding value in the BH case. The QNMs are functions of the parameter ϵ which is related to the compactness of the object. For $\epsilon \rightarrow 0$ we recover the fundamental BH QNM and axial and polar modes are isospectral, whereas for larger values of ϵ (less compact object) the QNMs differ from the BH case and isospectrality is broken. For large ζ or for $\epsilon \rightarrow 0$, the polar QNMs are independent of ζ . As a reference, the shaded regions correspond to the error bars (10% and 15%, respectively) on the frequency and the damping time for the merger event GW150914 [2, 11]. For $\epsilon \gtrsim 0.01$, these QNMs appear in the modified prompt ringdown, see e.g. Fig. 3.

reflections are strongly suppressed or absent, as in the bottom panel of Fig. 3.

B. QNM dependence on the compactness and viscosity

Let us first analyze the QNM spectrum of a dark compact object with $\eta = \eta_{\text{BH}}$. Figure 4 shows the real and imaginary part of the axial and polar QNMs as a function of ϵ , with respect to the BH case. As expected, for $\epsilon \rightarrow 0$ we recover the fundamental $l = 2$ QNM of a Schwarzschild BH, $M\omega_{\text{BH}} \approx 0.3737 - i0.089$. For larger values of ϵ , the compactness of the object decreases and the QNMs depart from the BH case. From the previous discussion, for $\epsilon \ll 0.01$ the (small) deviations to the QNMs do not affect the prompt ringdown. Furthermore, for $\eta = \eta_{\text{BH}}$ echoes are suppressed, so an object with $\epsilon \ll 0.01$ and $\eta = \eta_{\text{BH}}$ is indistinguishable from a BH in terms of its ringdown.

For $\epsilon \gtrsim 0.01$, the prompt ringdown is affected by the modified QNMs. Indeed, by fitting the time-domain waveform at late times with a damped sinusoid, $\Psi(t) \sim A \cos(\omega_R t + \phi) e^{-t/\tau}$, we can verify that in this range the prompt ringdown is governed by the *modified* fundamental QNM of the system. This noteworthy feature carries a characteristic imprint of the structure of the remnant.

The QNMs of the Schwarzschild BH enjoy a remarkable “isospectrality” [5, 90]: the entire spectrum is the same for the axial and the polar gravitational sectors. This isospectrality is broken for finite values of ϵ (and for $\eta \neq \eta_{\text{BH}}$, as discussed below). For each point of the parameter space, the $l = 2$ fundamental QNMs form a *doublet*.

Polar modes are qualitatively similar to the axial ones and show a mild dependence on the bulk viscosity ζ . The QNM spectrum is independent of ζ in the large- ζ limit, as shown in Fig. 4 by the $\zeta = \pm 10$ curves. This is expected since, when $\zeta \rightarrow \infty$, the polar boundary condition (12) is independent of ζ , and the second term of the right-hand side reduces to $G = \frac{3M(R-2M)}{R^2(3M+qR)}$.

Finally, Fig. 5 shows the complex QNM plane of a dark compact object for axial perturbations. For a given value of ϵ , each curve is parametrized by the shear viscosity⁶ η . As the location of the surface approaches the light ring ($\epsilon \rightarrow 1/2$), the axial QNMs become independent of η . Indeed, they tend to a universal mode which, for $l = 2$, reads

$$M\omega_{\text{axial}} \approx 0.3601 - i0.2149, \quad \epsilon \rightarrow 1/2, \quad (18)$$

for any value of η . As previously discussed, in this limit the object becomes a perfect reflector of axial GWs, regardless of the value of η . Therefore, a compact object with $R = 3M$ has a *universal axial QNM spectrum*, regardless of its properties (but see footnote 5 for a loophole). Unfortunately, this remarkable universality does not apply to the polar sector, since there does not exist a value of R at which the function G defined in Eq. (12) diverges for any value of η , ζ , and ω .

⁶ We focus on $\eta > 0$ because, consistently with the previous analysis of the reflectivity coefficient, when $\eta < 0$ we found *unstable* modes (i.e., modes with $\omega_I > 0$). This is expected since a negative shear viscosity corresponds to energy injected into the system, i.e., to a super-emitter with $|\mathcal{R}|^2 > 1$ [82].

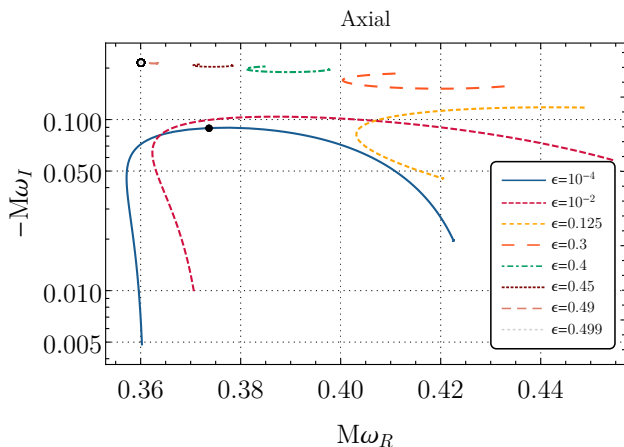


FIG. 5. The complex QNM plane for axial modes. Each curve is parametrized in terms of the effective shear viscosity $\eta \in [10^{-4}, 100]$. As $\epsilon \rightarrow 1/2$, the curves collapse to a single *universal* point (black empty circle), corresponding to the universal QNM in Eq. (18). As a reference, the fundamental QNM of a Schwarzschild BH is marked by a black dot.

C. Transition from fundamental modes to overtones & instability of the QNM spectrum

As previously discussed, the computation of the QNMs in the $\epsilon \rightarrow 0$ limit is less relevant from a phenomenological point of view, since these modes do not govern the prompt ringdown but only the late-time echo structure [17]. Nonetheless, from a theoretical standpoint it is enlightening to study their dependence on η , since this parameter interpolates between the BH limit ($\eta = \eta_{\text{BH}}$) and the perfectly reflecting case ($\eta \rightarrow 0, \infty$).

For concreteness, we consider $\epsilon = 10^{-10}$ and track the QNMs from the BH case ($\eta = \eta_{\text{BH}}$) down to $\eta = 0$. In Fig. 6, we show the imaginary part of the axial QNMs obtained with this procedure starting from the fundamental ($n = 0$, blue curve) mode and from its first overtone ($n = 1$, red curve). As expected, at the starting point we recover the modes of a Schwarzschild BH. However, immediately after η decreases (going on the right in the plot) there is a crossing point between the two curves: already when $\eta < 0.99997\eta_{\text{BH}}$ the first BH overtone becomes longer lived (i.e., smaller ω_I) than the fundamental BH mode, showing that the former becomes more relevant for the late-time dynamics of the system⁷. Although tracking higher overtones is challenging, we have indications that this behavior is rather general: higher overtones increasingly become more relevant in the $\eta \rightarrow 0$ limit.

⁷ Recently, it has been realized that the overtones might play an important role in the ringdown of loud mergers [91–97]. Studying the implication of our results for overtones is an interesting extension of this work.

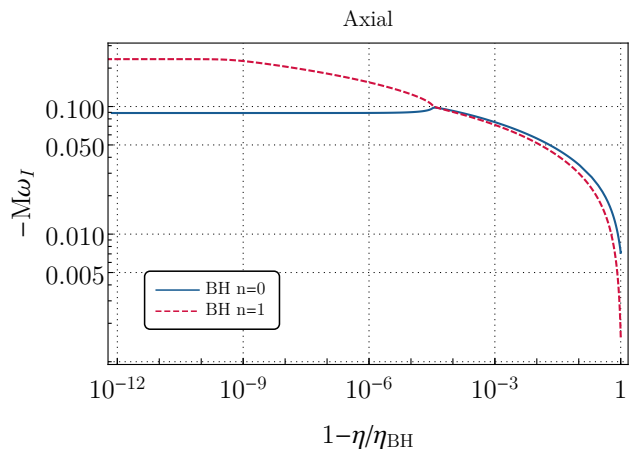


FIG. 6. Imaginary part of the axial QNMs of a dark compact object with radius $R = 2M(1 + \epsilon)$ and $\epsilon = 10^{-10}$ as a function of the effective shear viscosity, tracking the fundamental ($n = 0$, blue curve) and first overtone ($n = 1$, red curve) QNM of a Schwarzschild BH (leftmost part of the plot) down to the limit of perfectly reflecting object ($\eta = 0$, rightmost part). There exists a crossing point at which the imaginary part of the BH overtone becomes smaller than that of the BH fundamental mode. The polar case is qualitatively similar.

Indeed, neither of the modes shown in Fig. 6 for $\eta \rightarrow 0$ correspond to the fundamental mode of the perfectly reflecting case. The latter is a long-lived mode with a tiny imaginary part [81]. Interestingly enough, tracking the fundamental mode from the perfectly reflecting case back to η_{BH} is extremely challenging. We suspect that this is connected to the fact that – when tracked to $\eta \rightarrow \eta_{\text{BH}}$ – this mode corresponds to a very high-order overtone in the BH limit, which are extremely difficult to compute numerically, due to their large imaginary part. Furthermore, an interesting property of the BH QNM spectrum is its instability against small deformations of the eigenvalue problem, such as bumps in the effective potential [98–100] or slightly different boundary conditions [38] (see Ref. [101] for recent work on this topic). In our numerical analysis we have seen hints of this instability (which is more severe for high-order overtones [101]) due to finite- ϵ effects and to the slightly different boundary conditions when approaching the BH limit. We defer a detailed analysis of this interesting problem to the future, stressing that our framework is well-suited to explore this problem in full generality.

D. Detectability

Figure 7 shows the relative percentage difference between the BH QNM and the QNMs of a dark compact object in the (ϵ, η) parameter space. Based on the previous discussion, we focus on the region which directly affects the prompt ringdown, i.e., $\epsilon \gtrsim \mathcal{O}(0.01)$ and $\eta \in [0, \eta_{\text{BH}}]$.

As a reference, in Fig. 7 we show the contour lines

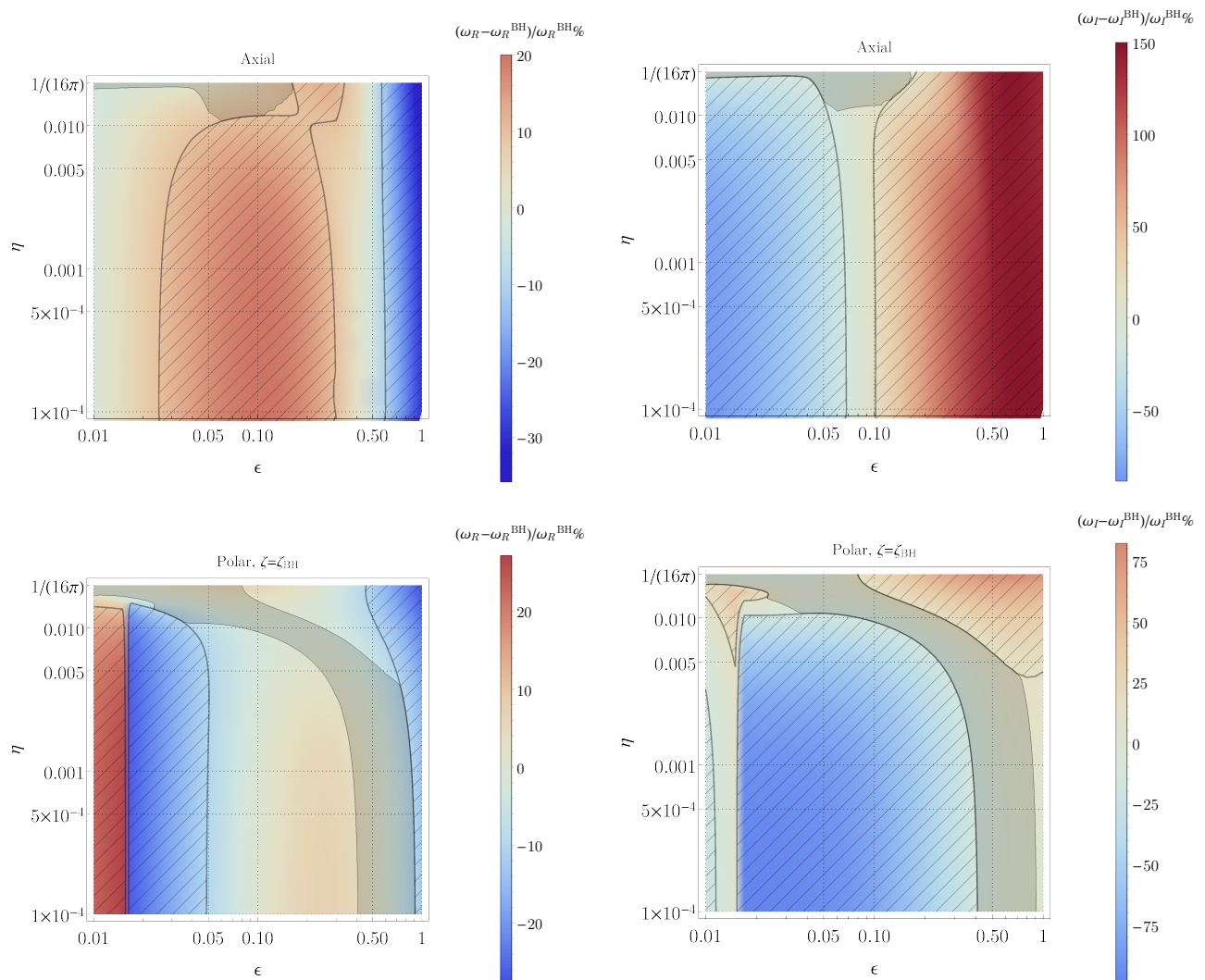


FIG. 7. Relative percentage difference of the real (left panel) and imaginary (right panel) part of the gravitational $l = 2$ QNMs of a dark compact object with respect to the BH QNM. The difference is parametrized by the shear viscosity $\eta \in [0, \eta_{\text{BH}}]$ of a fictitious fluid located at $R = 2M(1 + \epsilon)$ and by the compactness of the object through the parameter $\epsilon \in [0.01, 1]$. As a reference, the contour lines correspond to the accuracy in the measurement of the fundamental QNM of GW150914 and the dashed areas are the regions of the parameter space potentially excluded by individual measurements of ω_R (left) or ω_I (right). The dark shaded region in all panels is the area not excluded by a simultaneous measurement of the frequency and the damping time with the same accuracy as GW150914.

corresponding to 10% and 15% of relative difference for ω_R and ω_I , respectively, which roughly correspond to the accuracy within which the fundamental QNM of the remnant in GW150914 has been measured. Although in the latter case the remnant is spinning [11], we can assume $\approx (10 - 15)\%$ as an approximate estimate for the ring-down resolution of LIGO/Virgo for “golden” events such as GW150914. For the same type of events, an overall improvement of the signal-to-noise ratio by an order of magnitude will provide a resolution at the percent level.

Measuring a single mode in the ringdown only allows to extract the mass and the spin of the object and one would need to measure at least two QNMs to verify whether

the QNM spectrum is compatible with a BH in General Relativity. However, independent estimates of the mass and spin can be extracted from the inspiral-merger signal, assuming a binary BH in General Relativity [2, 11]. Any deviation from the expected fundamental QNM would imply a failure of this test, suggesting either a departure from General Relativity or that the remnant is not a Kerr BH, or both.

Interestingly, already with the current LIGO/Virgo accuracy one can potentially place very strong constraints on the parameter space of our model, excluding the regions of the parameter space hatched in Fig. 7. By combining the information from the real and the imaginary

part of the QNMs, Fig. 7 shows that only a small region of the parameter space with $\epsilon \lesssim 0.1$ and $\eta \sim \eta_{\text{BH}}$ (dark shaded area) is compatible with the current constraints for both axial and polar perturbations. For polar perturbations, also a region with $\epsilon \gtrsim 0.1$ and $0 < \eta < \eta_{\text{BH}}$ is compatible with the current constraints. Our results suggest that an improvement by a factor of a few in the detector sensitivity relative to LIGO first observational run would firmly rule out any modification of the prompt ringdown in our model.

Furthermore, as previously discussed, a generic feature of departure from the BH picture is the presence of a mode doublet. The frequencies of axial and polar modes are similar in most of the parameter space, with some regions featuring relative differences as large as $\approx 40\%$; however, the relative difference of the damping times can be much bigger (as large as $\approx 1500\%$ in some regions). A necessary condition for resolving these differences is based on the Rayleigh resolvability criterion [8, 93]

$$\max[\sigma_{f_1}, \sigma_{f_2}] < |f_1 - f_2|, \quad (19)$$

$$\max[\sigma_{Q_1}, \sigma_{Q_2}] < |Q_1 - Q_2|, \quad (20)$$

where $f_i = \omega_R^{(i)}/(2\pi)$ and $Q_i = \pi f_i \tau_i$ are the frequency and quality factor of the i -th mode, and σ_X is the uncertainty in recovering a quantity X . In Fig. 8 we show the minimum signal-to-noise ratio, ρ_{res} , required to resolve the axial and polar QNMs according to the above criterion. We computed the uncertainties on the parameters with a simple Fisher analysis [8, 93] adapted from the case of BH overtones [95, 97], and assuming that the amplitude ratio between the axial and polar modes is $1/10$. In the $\eta \approx \eta_{\text{BH}}$ region $\rho_{\text{res}} > 10^3$, but it can be much smaller for $\eta < \eta_{\text{BH}}$. Although, a comparison between Fig. 8 and Fig. 7 shows that detecting deviations from the BH QNMs should require a much smaller signal-to-noise ratio than resolving the axial-polar doublet, the existence of this doublet is a generic smoking gun of objects other than BHs, so it might be useful to place model-independent constraints.

Finally, let us look at the opposite regime, where $\epsilon \ll 0.01$. In this case the prompt ringdown is not modified and the constraints on the model rely on the detectability of the echoes. This problem has been recently analyzed in detail [41, 55–57, 59–62, 67, 68]. In particular, Refs. [61, 62] analyzed the detectability as a function of the intrinsic reflectivity of the object, which coincides with Eq. (16) at high frequencies. By using the latter equation, we can map previous constraints on the object's reflectivity to the viscosity parameter. In particular, using the results of Refs. [61, 62], our analysis suggests that echoes are detectable with current GW interferometers at 2σ confidence level if $\eta < 0.06\eta_{\text{BH}}$. Future detectors such as the Einstein Telescope [102] and LISA [103] will allow to probe $\eta < 0.4\eta_{\text{BH}}$ and $\eta < 0.6\eta_{\text{BH}}$, respectively, at the same confidence level, while future LISA+ concepts [104] can reach almost $\eta \approx \eta_{\text{BH}}$ at 3σ level. In other words, current GW interferometers could detect echoes only if the effective viscosity of the object is at most 6% of that

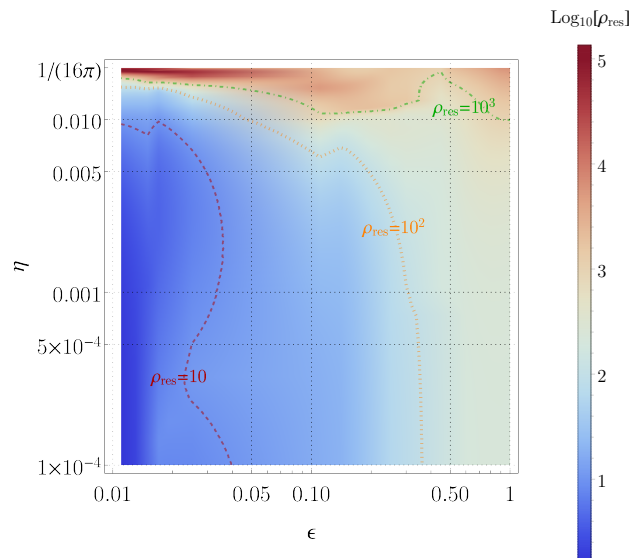


FIG. 8. Minimum signal-to-noise ratio required for the resolvability of the axial-polar QNM doublet according to the Rayleigh criterion.

of a BH, larger values of η would result in echoes that are too damped to be detectable with current facilities.

IV. CONCLUDING REMARKS

If an object is almost as compact as a BH and absorbs radiation almost as much as BH, then its QNM spectrum is almost indistinguishable from that of a BH. Besides confirming this reasonable expectation, our analysis provides a general framework to quantify the next natural question: *when does the ringdown of a dark compact object become distinguishable from that of a BH?*

If an object with radius $R = 2M(1 + \epsilon)$ is sufficiently compact ($\epsilon \ll 0.01$), the prompt ringdown is universal and the properties of the object's interior can appear only after the scrambling time $\tau_{\text{echo}} \sim M |\log \epsilon|$ [38–40], provided that the viscosity is sufficiently small. Thus, a negative echo search places an upper bound on the viscosity of the model, with current (future) detectors being able to probe values of η as large as 6% (60%) of the BH viscosity.

For less compact objects ($\epsilon \gtrsim 0.01$), there are no repeated echoes but the prompt ringdown is affected by the properties of the object's interior. In particular, the late-time ringdown is governed by the modified QNMs of the system. When the object is a perfect absorber at high frequency ($\eta = \eta_{\text{BH}}$) the fundamental QNM deviates as much as $\mathcal{O}(10\%)$ and $\mathcal{O}(100\%)$ (for the real and imaginary part, respectively) from the BH case when $\epsilon = \mathcal{O}(0.1)$. Although a more refined analysis is needed (in particular including the spin of the object), this suggests that inspiral-merger-ringdown consistency

tests [2, 3] can already put a strong constraint on ϵ of the order of $\epsilon \lesssim 0.01$, i.e., the compactness of the remnant cannot be smaller than 99% that of a BH (see Fig. 7). Future ringdown detections have the capability to rule out any deviation of the prompt ringdown in our model.

A generic feature that emerges from our framework is the fact that objects with $\epsilon \gtrsim \mathcal{O}(0.1)$ have a significant reflectivity at the typical ringdown frequency (even when $\eta = \eta_{\text{BH}}$) compared to the BH case. This enhances the effects of the object's interior in the ringdown. This phenomenon is most dramatic in the axial case, when the QNM spectrum becomes independent of η as $\epsilon \rightarrow 1/2$ and the reflectivity is unity. An object with radius equal to the light ring becomes a *perfect reflector* of axial GWs and its axial QNM spectrum is universal.

Another generic feature is the breaking of isospectrality. Axial and polar modes are generically different except for the measure-one subspace ($\epsilon \rightarrow 0$, $\eta = \eta_{\text{BH}}$) of the whole three-dimensional (ϵ, η, ζ) parameter space. Assuming that axial and polar modes are excited with comparable amplitude during the merger, this implies that a dark object other than a BH should vibrate with a mode *doublet*. Resolving these doublet when $\eta \approx \eta_{\text{BH}}$ requires a signal-to-noise ratio in the ringdown signal above 10^3 , whereas it takes much smaller sensitivity in other regions of the parameter space.

Our framework can be applied to specific models of extreme compact objects [17], such as wormholes [105], gravastars [83, 84, 106, 107], superspinars [108], nonlocal stars [28], and horizonless microstate geometries [23–27]. In specific models the viscosity parameters might be complex and frequency dependent. This extension should be straightforward and is left for the future.

Likewise, we focused on nonrotating objects for simplicity, but our approach is conceptually valid also in the case of rotation. In that case, we envisage two technical obstacles: (i) the junction conditions require the analysis of metric perturbations, which should therefore be reconstructed from the Teukolsky function [109, 110]; (ii) the absence of Birkhoff's theorem in axisymmetry implies that the exterior of the object is not necessarily described by the Kerr metric. While deviations might be small in the $\epsilon \rightarrow 0$ limit [111], when $\epsilon = \mathcal{O}(0.1 - 1)$ a case-by-case analysis might be required. In the spinning case, it would also be interesting to study the ergoregion instability [112–114] and how the latter can be quenched in particular models [42, 77, 81].

ACKNOWLEDGMENTS

The authors are grateful to Emanuele Berti for useful correspondence on the continued fraction method for stars, and to Samir Mathur, Gabriel Andres Piovano, Guilherme Raposo, and Lucas Tonetto for useful discussions. L.B. thanks Sapienza University of Rome for the hospitality in the first stages of this project. L.B. acknowledges financial support from JSPS

and KAKENHI Grant-in-Aid for Scientific Research No. JP19F19164. P.P. and E.M. acknowledge financial support provided under the European Union's H2020 ERC, Starting Grant agreement no. DarkGRA–757480, under the MIUR PRIN and FARE programmes (GW-NEXT, CUP: B84I20000100001), and support from the Amaldi Research Center funded by the MIUR program “Dipartimento di Eccellenza” (CUP: B81I18001170001). A.M. is supported by Netherlands Organization for Scientific Research (NWO) Grant number 680-91-119.

Appendix A: Membrane paradigm

In this appendix we provide details on the computation leading to the boundary conditions (11) and (12). Let \mathcal{M} be the whole spacetime manifold. We can define a 3-dimensional spherical membrane (or shell) generated by time-like geodesics of radius $R = 2M(1 + \epsilon)$, whose interior \mathcal{M}^- and exterior \mathcal{M}^+ regions are described by two different metrics $g_{\mu\nu}^-(x^-)$ and $g_{\mu\nu}^+(x^+)$, respectively, with x^\pm being the respective coordinates. The exterior region is described by the Schwarzschild metric (2). The two sets of coordinates are

$$x^{-\mu} = (t^-, r^-, \theta^-, \varphi^-), \quad x^{+\mu} = (t^+, r^+, \theta^+, \varphi^+), \quad (\text{A1})$$

while the membrane's coordinates are $x_m^\mu = (t, R, \theta, \varphi)$, so that the intrinsic 3-dimensional coordinates on the shell are

$$y^a = (t, \theta, \varphi). \quad (\text{A2})$$

The normal vector n^μ to the time-like membrane is space-like, i.e., $n_\mu n^\mu = 1$. A basis of three independent generators for the shell can be chosen as

$$e_a^\mu = \frac{\partial x^\mu}{\partial y^a}, \quad (\text{A3})$$

through which we can define the induced metric

$$h_{ab} = e_a^\mu e_b^\nu g_{\mu\nu}. \quad (\text{A4})$$

on the 3-dimensional surface. The extrinsic curvature on the membrane is defined as

$$K_{ab} = e_a^\mu e_b^\nu \nabla_\mu n_\nu, \quad (\text{A5})$$

and its trace is $K = h^{ab} K_{ab}$. To embed the 3-dimensional membrane in the manifold \mathcal{M} we need to impose a junction condition that glues the interior region with the exterior [73]:

$$(K^+ h_{ab} - K_{ab}^+) - (K^- h_{ab} - K_{ab}^-) = 8\pi T_{ab}, \quad (\text{A6})$$

where K_{ab}^+ and K_{ab}^- are the extrinsic curvatures defined on the top and on the bottom of the shell, respectively; T_{ab} is the stress-energy tensor of some matter distribution located on the membrane creating a discontinuity in the extrinsic curvature.

The crucial and fundamental assumption of the membrane paradigm is that such a stress-energy tensor is fictitious and its role is to carry all the information about the interior. In the standard paradigm, one assumes that the inside region is such that

$$K_{ab}^- = 0, \quad (\text{A7})$$

so that the junction condition (A6) reduces to [37]

$$K h_{ab} - K_{ab} = 8\pi T_{ab}, \quad (\text{A8})$$

where for simplicity we have redefined $K_{ab} \equiv K_{ab}^+$, and henceforth we denote the coordinates outside simply as $x^\mu = (t, r, \theta, \varphi)$.

The junction conditions are compatible with the stress-energy tensor of a dissipative fluid, Eq. (4), where ρ and p are the density and pressure, respectively; u_a is the 3-velocity of the fluid defined in terms of its 4-velocity U_μ as $u_a = e_a^\mu U_\mu$. Moreover, $\Theta = u_{;a}^a$ is the expansion, $\sigma_{ab} = \frac{1}{2}(u_{a;c}\gamma_b^c + u_{b;c}\gamma_a^c - \Theta\gamma_{ab})$ is the shear tensor, where $\gamma_{ab} = h_{ab} + u_a u_b$ is the projector tensor, and $u_{b;a}$ is the 3-dimensional covariant derivative compatible with the induced metric h_{ab} [115, 116].

1. Unperturbed background

In the static background [Eq. (2)] the viscosity parameters η and ζ do not play any role. Indeed, it is easy to show that the expansion and shear are zero, so the membrane stress-energy tensor reduces to that of a perfect fluid. In this case, the 3-metric reads

$$h_{tt} = -f(R), \quad h_{\theta\theta} = \frac{h_{\varphi\varphi}}{\sin^2\theta} = R^2. \quad (\text{A9})$$

The normal vector n^μ can be uniquely determined by imposing the four conditions $n^\mu n_\mu = 1$ and $e_a^\mu n_\mu = 0$; its components read

$$n_t = 0, \quad n_r = \frac{1}{\sqrt{f(r)}}, \quad n_\theta = 0, \quad n_\varphi = 0. \quad (\text{A10})$$

The extrinsic curvature is also diagonal,

$$K_{tt} = -\frac{1}{2}\sqrt{f(R)}f'(R), \quad K_{\theta\theta} = \frac{K_{\varphi\varphi}}{\sin^2\theta} = R\sqrt{f(R)},$$

where a prime denotes partial derivative with respect to the argument.

The only nonvanishing component of the fluid 4-velocity $U^\mu = (U^t, U^r, U^\theta, U^\varphi)$ is $U^t = 1/\sqrt{f(R)}$. This yields the 3-velocity

$$u_a = e_a^\mu U_\mu, \quad u^a = h^{ab}u_b = \left(\frac{1}{\sqrt{f(R)}}, 0, 0\right). \quad (\text{A11})$$

Therefore, the nonvanishing components of the junction condition (A8) at the background level are

$$tt : -\frac{2}{R}f^{3/2}(R) = 8\pi f(R)\rho_0,$$

$$\begin{aligned} \theta\theta : \frac{R(2f(R) + Rf'(R))}{2\sqrt{f(R)}} &= 8\pi R^2 p_0, \\ \varphi\varphi : \frac{R\sin^2\theta(2f(R) + Rf'(R))}{2\sqrt{f(R)}} &= 8\pi R^2 \sin^2\theta p_0. \end{aligned} \quad (\text{A12})$$

The (tt) component gives the unperturbed density of the membrane [69]

$$\rho_0(R) = -\frac{\sqrt{f(R)}}{4\pi R}, \quad (\text{A13})$$

while the angular components give the unperturbed pressure of the membrane

$$p_0(R) = \frac{2f(R) + Rf'(R)}{16\pi R\sqrt{f(R)}}. \quad (\text{A14})$$

The speed of sound is

$$c_s \equiv \sqrt{\frac{\partial p_0}{\partial \rho_0}} = \sqrt{\frac{1 + 2\epsilon + 4\epsilon^2}{8\epsilon(1/2 - \epsilon)}}, \quad (\text{A15})$$

which diverges as $\epsilon \rightarrow 0, 1/2$ and is complex for $\epsilon > 1/2$. Note, however, that the properties of the fluid do not need to be physical, since the membrane is fictitious.

2. Gravitational perturbations

We work in the Regge-Wheeler gauge [78] and study separately the axial and polar sectors of gravitational perturbations, since they decouple in presence of a static background.

The perturbed metric can be cast in the following general form

$$g_{\mu\nu} = g_{\mu\nu}^0(r) + \delta g_{\mu\nu}(r, \theta, t), \quad (\text{A16})$$

where, without loss of generality, the perturbation $\delta g_{\mu\nu}$ does not depend on the azimuthal angle φ , owing to the spherical symmetry of the background $g_{\mu\nu}^0$.

Because of the metric perturbations, the dissipative components of the stress-energy tensor are switched on, and both density and pressure are perturbed as follows

$$\rho = \rho_0 + \delta\rho(t, \theta), \quad (\text{A17})$$

$$p = p_0 + \delta p(t, \theta). \quad (\text{A18})$$

Also the location of the membrane is affected by the perturbation, and we can parametrize the deviation as

$$r_m(t, \theta) = R + \delta R(t, \theta). \quad (\text{A19})$$

We can also easily find the expressions of the perturbed tangential vectors e_a^μ introduced in Eq. (A3). Since the 4-dimensional coordinates of the membrane are

$$x_m^\mu = (t, R + \delta R(t, \theta), \theta, \varphi), \quad (\text{A20})$$

we have

$$\begin{aligned} e_t^\mu &= (1, \partial_t \delta R(t, \theta), 0, 0) , \\ e_\theta^\mu &= (0, \partial_\theta \delta R(t, \theta), 1, 0) , \\ e_\varphi^\mu &= (0, 0, 0, 1) . \end{aligned} \quad (\text{A21})$$

Note that, $\delta\rho(t, \theta)$, $\delta p(t, \theta)$ and $\delta R(t, \theta)$ are scalar quantities under rotation, so they are only affected by polar perturbations and can be decomposed as

$$\begin{aligned} \delta\rho(t, \theta) &= \varepsilon \rho_1 P_l(\cos\theta) e^{-i\omega t} , \\ \delta p(t, \theta) &= \varepsilon p_1 P_l(\cos\theta) e^{-i\omega t} , \\ \delta R(t, \theta) &= \varepsilon \delta R_0 P_l(\cos\theta) e^{-i\omega t} . \end{aligned} \quad (\text{A22})$$

where ρ_1 , p_1 , δR_0 only depend on the unperturbed radius R , $P_l(\cos\theta)$ are the Legendre polynomials⁸ and the parameter ε keeps track of the order in perturbation, so that all contributions of order $\mathcal{O}(\varepsilon^2)$ are negligible.

In the following we treat the axial and polar sectors separately.

a. Axial sector

The nonvanishing components of the axial metric perturbations in the Regge-Wheeler gauge [78] are

$$\begin{aligned} \delta g_{t\varphi} &= \varepsilon e^{-i\omega t} h_0(r) \sin\theta \partial_\theta P_l(\cos\theta) , \\ \delta g_{r\varphi} &= \varepsilon e^{-i\omega t} h_1(r) \sin\theta \partial_\theta P_l(\cos\theta) . \end{aligned} \quad (\text{A23})$$

It follows that the only nonvanishing component of the 3-metric perturbation δh_{ab} is

$$\delta h_{t\varphi} = \varepsilon e^{-i\omega t} h_0(R) \sin\theta \partial_\theta P_l(\cos\theta) . \quad (\text{A24})$$

In the case of axial perturbations the the four components of the normal vector up to $\mathcal{O}(\varepsilon)$ are simply given by the unperturbed one in Eq. (A10). As a consequence, the nonvanishing components of the extrinsic curvature perturbation are

$$\begin{aligned} \delta K_{t\varphi} &= \frac{1}{2} e^{-i\omega t} \varepsilon \sqrt{f} (i\omega h_1 + h'_0) \sin\theta \partial_\theta P_l(\cos\theta) , \\ \delta K_{\theta\varphi} &= -\frac{1}{2} e^{-i\omega t} \varepsilon \sqrt{f} h_1 (\cos\theta \partial_\theta + \sin\theta \partial_\theta^2) P_l(\cos\theta) . \end{aligned}$$

As for the fluid velocity, the components U^t , U^r and U^θ are not affected by axial perturbations, while $\delta u^\varphi \neq 0$ and its expression can be found by solving the $(t\varphi)$ component of the junction condition,

$$\delta u^\varphi = \frac{\varepsilon e^{-i\omega t} \partial_\theta P_l(\cos\theta) [h_0 f' - f(i\omega h_1 + h'_0)]}{R \sin\theta \sqrt{f} (2f - Rf')} . \quad (\text{A25})$$

⁸ Note that we can set $m = 0$ in the spherical harmonics $Y_l^m(\theta, \varphi) \propto e^{im\varphi} P_l^m(\cos\theta)$ without any loss of generality due to the spherical symmetry of the background.

The perturbed components of the stress-energy tensor are

$$\begin{aligned} \delta T_{t\varphi} &= -\varepsilon e^{-i\omega t} \rho_0 h_0 \sin\theta \partial_\theta P_l(\cos\theta) \\ &\quad + R^2 \sqrt{f} \sin^2\theta (p_0 + \rho_0) \delta u^\varphi(t, \theta) , \\ \delta T_{\theta\varphi} &= -\varepsilon R^2 \sin^2\theta \partial_\theta \delta u^\varphi(t, \theta) . \end{aligned} \quad (\text{A26})$$

The $(\theta\varphi)$ component of the junction condition then reduces to

$$\frac{1}{2} \sqrt{f} h_1 = \frac{8\pi\eta R [h_0 f' - f(i\omega h_1 + h'_0)]}{\sqrt{f} (2f - Rf')} . \quad (\text{A27})$$

In vacuum the Regge-Wheeler functions are related to each other [78], $h_0(r) = -\frac{f(r)}{i\omega} \frac{d}{dr} [f(r) h_1(r)]$. One can use this relation to eliminate $h_0(R)$ and $h'_0(R)$ in terms of $h_1(R)$, $h'_1(R)$ and $h''_1(R)$. Furthermore, one can replace h_1 and its derivatives by introducing the Regge-Wheeler function,

$$\psi(r) = \frac{f(r)}{r} h_1(r) \quad (\text{A28})$$

which satisfies Eq. (6) with effective potential V_{axial} . We finally obtain

$$\omega\psi(R) = i16\pi\eta \left(\frac{\partial\psi}{\partial x} \Big|_R + \frac{RV_{\text{axial}}(R)}{2f(R) - Rf'(R)} \psi(R) \right) . \quad (\text{A29})$$

which coincides with Eq. (11) in the main text.

b. Polar sector

The nonvanishing components of the polar metric perturbation are

$$\begin{aligned} \delta g_{tt} &= \varepsilon e^{-i\omega t} P_l(\cos\theta) f(r) \mathcal{H}(r) , \\ \delta g_{rr} &= \varepsilon e^{-i\omega t} P_l(\cos\theta) \frac{\mathcal{H}(r)}{f(r)} , \\ \delta g_{tr} &= \varepsilon e^{-i\omega t} P_l(\cos\theta) \mathcal{H}_1(r) , \\ \delta g_{\theta\theta} &= \frac{\delta g_{\varphi\varphi}}{\sin^2\theta} = \varepsilon e^{-i\omega t} P_l(\cos\theta) r^2 \mathcal{K}(r) , \end{aligned} \quad (\text{A30})$$

and the location of the membrane is perturbed as in Eq. (A22).

By projecting on the 3-dimensional membrane, the nonvanishing components of the 3-metric perturbation δh_{ab} read

$$\begin{aligned} \delta h_{tt} &= \varepsilon (f\mathcal{H} - f'\delta R_0) P_l(\cos\theta) e^{-i\omega t} , \\ \delta h_{\theta\theta} &= \frac{h_{\varphi\varphi}}{\sin^2\theta} = \varepsilon (R^2\mathcal{K} + 2R\delta R_0) P_l(\cos\theta) e^{-i\omega t} . \end{aligned} \quad (\text{A31})$$

Moreover, the perturbed components of the normal vector for polar perturbations up to first order in ε are

$$\delta n_t = \frac{\varepsilon i\omega e^{-i\omega t} P_l(\cos\theta) \delta R_0}{\sqrt{f(r)}} ,$$

$$\begin{aligned}\delta n_r &= \frac{\varepsilon e^{-i\omega t} P_l(\cos\theta) \mathcal{H}(r)}{2\sqrt{f(r)}}, \\ \delta n_\theta &= -\frac{\varepsilon e^{-i\omega t} \partial_\theta P_l(\cos\theta) \delta R_0}{\sqrt{f(r)}}.\end{aligned}\quad (\text{A32})$$

As for the perturbed fluid velocity, in the polar sector δU^t can be uniquely determined from the condition on the norm $U_\mu U^\mu = -1$,

$$\delta U^t = \delta u^t = \frac{\varepsilon (f\mathcal{H} - \delta R_0 f')}{2f^{3/2}} P_l(\cos\theta) e^{-i\omega t}.\quad (\text{A33})$$

We can now compute the polar perturbation in the extrinsic curvature whose nonvanishing components up to first order in ε are

$$\begin{aligned}\delta K_{tt} &= \frac{\varepsilon e^{-i\omega t} P_l(\cos\theta) \left[\delta R_0 (4\omega^2 - f'^2) + f (-2\delta R_0 f'' + 3\mathcal{H}f' + 4i\omega\mathcal{H}_1) + 2f^2\mathcal{H}' \right]}{4\sqrt{f}}, \\ \delta K_{\theta\theta} &= \frac{\varepsilon e^{-i\omega t} \left[f (2\delta R_0 - R\mathcal{H} + R^2\mathcal{K}' + 2R\mathcal{K}) + \delta R_0 (Rf' - 2\partial_\theta^2) \right] P_l(\cos\theta)}{2\sqrt{f}}, \\ \delta K_{\varphi\varphi} &= \frac{\varepsilon \sin^2\theta e^{-i\omega t} \left[f (2\delta R_0 - R\mathcal{H} + R^2\mathcal{K}' + 2R\mathcal{K}) + \delta R_0 (Rf' - 2\cot\theta\partial_\theta) \right] P_l(\cos\theta)}{2\sqrt{f}}, \\ \delta K_{t\theta} &= -\frac{\varepsilon e^{-i\omega t} \partial_\theta P_l(\cos\theta) (f\mathcal{H}_1 - 2i\delta R_0\omega)}{2\sqrt{f}}.\end{aligned}\quad (\text{A34})$$

The nonvanishing components of the perturbation to the stress-energy tensor are

$$\begin{aligned}\delta T_{tt} &= \varepsilon e^{-i\omega t} P_l(\cos\theta) [\rho_0 f' \delta R_0 + f(\rho_1 - \rho_0 \mathcal{H})], \\ \delta T_{\theta\theta} &= \frac{R}{\sqrt{f}} \left\{ -\sqrt{f} R [(\zeta + \eta) \partial_\theta \delta u^\theta + (\zeta - \eta) \cot\theta \delta u^\theta] \right. \\ &\quad \left. + \varepsilon e^{-i\omega t} P_l(\cos\theta) \left[\sqrt{f} (p_0 R\mathcal{K} + 2p_0 \delta R_0 + p_1 R) + i\zeta\omega (R\mathcal{K} + 2\delta R_0) \right] \right\}, \\ \delta T_{\varphi\varphi} &= \frac{R \sin^2\theta}{\sqrt{f}} \left\{ -\sqrt{f} R [(\zeta - \eta) \partial_\theta \delta u^\theta + (\zeta + \eta) \cot\theta \delta u^\theta] \right. \\ &\quad \left. + \varepsilon e^{-i\omega t} P_l(\cos\theta) \left[\sqrt{f} (p_0 R\mathcal{K} + 2p_0 \delta R_0 + p_1 R) + i\zeta\omega (R\mathcal{K} + 2\delta R_0) \right] \right\}, \\ \delta T_{t\theta} &= -R^2 \sqrt{f} (\rho_0 + p_0) \delta u^\theta.\end{aligned}\quad (\text{A35})$$

From the components (tt) , $(\theta\theta)$, and $(\varphi\varphi)$ of the junction conditions we obtain analytical (albeit cumbersome) expressions for ρ_1 and p_1 , and the deviation in the membrane location

$$\delta R_0 = \frac{16\pi\eta R f \mathcal{H}_1}{2f - Rf' - 32\pi\eta i\omega R},\quad (\text{A36})$$

whereas from the $(t\theta)$ component we derive

$$\delta u^\theta = \frac{\varepsilon e^{-i\omega t} \partial_\theta P_l(\cos\theta) R \sqrt{f} \mathcal{H}_1}{2f - Rf' - 32\pi\eta i\omega R}.\quad (\text{A37})$$

This still leaves the metric perturbations, $\mathcal{H}(r)$, $\mathcal{H}_1(r)$ and $\mathcal{K}(r)$, unknown. In vacuum, these three functions are related by the following algebraic equation [79, 80]:

$$\mathcal{H}(r) = \frac{1}{qr + 3M} \left\{ \left[qr - \frac{\omega^2 r^4}{r - 2M} + M \frac{r - 3M}{r - 2M} \right] \mathcal{K}(r) \right.$$

Moreover, $\delta U^\varphi = \delta u^\varphi = 0$ and $\delta U^r = -\varepsilon U^t i\omega e^{-i\omega t} P_l(\cos\theta)$, while $\delta U^\theta = \delta u^\theta$ is nonvanishing and can be determined by solving the $(t\theta)$ component of the junction condition (A8), as we will see below.

$$\left. + \left[i\omega r^2 + \frac{(q+1)M}{i\omega r} \right] \mathcal{H}_1(r) \right\},\quad (\text{A38})$$

where $q = (l-1)(l+2)/2$. The last relation allows us to eliminate, say, $\mathcal{H}(r)$.

Moreover, we can rewrite $\mathcal{H}_1(r)$ and $\mathcal{K}(r)$ in terms of the Zerilli function $Z(x)$, which satisfies Eq. (6) with $V = V_{\text{polar}}$ [79, 80]. Indeed,

$$\mathcal{H}_1(r) = \omega h(r) Z(x) + \omega k(r) \frac{dZ(x)}{dx},\quad (\text{A39})$$

$$\mathcal{K}(r) = g(r) Z(x) + \frac{dZ(x)}{dx},\quad (\text{A40})$$

where [79, 80]

$$h(r) = i \frac{3qMr - qr^2 + 3M^2}{(r-2M)(qr+3M)},$$

$$k(r) = -i \frac{r^2}{r - 2M},$$

$$g(r) = \frac{q(q+1)r^2 + 3qMr + 6M^2}{r^2(qr + 3M)}. \quad (\text{A41})$$

The last condition which closes the system of equations and uniquely determines the boundary conditions for the polar metric perturbations at $r = R$ is found from the barotropic equation of state $p = p(\rho)$, at first order in perturbation, which gives

$$\delta p = c_s^2 \delta \rho, \quad (\text{A42})$$

where the sound speed squared is given by Eq. (A15).

By substituting the above algebraic equations, after a tedious but conceptually simple calculation we obtain the following boundary condition

$$\frac{\partial_x Z(x)}{Z(x)} = -16\pi\eta\omega + G(R, \omega, \eta, \zeta), \quad (\text{A43})$$

where $G = A/B$ and

$$A = (y - 2) \left\{ 9 \left[-3 - 3w^2y^3 + w^2y^4 - 48i\pi w y^2 \zeta + y(2 + 96i\pi w \zeta) \right] + q^3 y^2 (-3i + iy + 16\pi w y^2 \eta)^2 \right. \\ \left. + 3q \left[-9 + 3y^2(1 + 64i\pi w \zeta) - 32i\pi w y^3(3\zeta + 2\eta) + w y^4(-3w + 16i\pi \eta) + w^2 y^5(1 + 256\pi^2 \eta^2) \right] \right. \\ \left. + q^2 y \left[-18 + 6y^2(1 + 16i\pi w(\zeta - 2\eta)) + 256\pi^2 w^2 y^5 \eta^2 + 32\pi w y^4 \eta(i + 24\pi w \eta) - iy^3(-i + 48\pi w(\zeta + \eta)) \right] \right\}, \quad (\text{A44})$$

$$B = y^2(3 + qy) \left\{ 3 \left[-3 - 3w^2y^3 + w^2y^4 - 48i\pi w y^2 \zeta + y(2 + 96i\pi w \zeta) \right] \right. \\ \left. + q \left[-9 + 9y + w^2 y^5 + y^2(-3 + 192i\pi w \zeta) + y^3(1 - 32i\pi w(3\zeta - \eta)) - w y^4(3w + 16i\pi \eta) \right] \right. \\ \left. + q^2 y \left[3 - 3y - 16i\pi w y^3(\zeta + \eta) + y^2(1 + 32i\pi w(\zeta + \eta)) \right] \right\}, \quad (\text{A45})$$

and we have defined the dimensionless quantities $y = R/M$, $w = M\omega$. Note that in the BH limit $G(2M) = 0$, and the BH boundary condition is recovered for $\eta = 1/(16\pi)$, consistently with the axial case.

density ρ and the expansion Θ vanish for a perturbed Schwarzschild spacetime. In the BH limit the effective stress-energy tensor (4) reduces to

$$T_{ab}^{\text{BH}} = p\gamma_{ab} - 2\eta_{\text{BH}}\sigma_{ab}, \quad R \rightarrow 2M, \quad (\text{A46})$$

Finally, from our computations it follows that both the

which is independent of ζ , as discussed in the main text.

-
- [1] W. E. Lamb and R. C. Retherford, “Fine structure of the hydrogen atom by a microwave method,” *Phys. Rev.* **72** (Aug, 1947) 241–243. <https://link.aps.org/doi/10.1103/PhysRev.72.241>.
- [2] **LIGO Scientific, Virgo Collaboration**, B. Abbott *et al.*, “Tests of general relativity with GW150914,” *Phys. Rev. Lett.* **116** no. 22, (2016) 221101, [arXiv:1602.03841](https://arxiv.org/abs/1602.03841) [gr-qc]. [Erratum: *Phys.Rev.Lett.* 121, 129902 (2018)].
- [3] **LIGO Scientific, Virgo Collaboration**, B. Abbott *et al.*, “Tests of General Relativity with the Binary Black Hole Signals from the LIGO-Virgo Catalog GWTC-1,” *Phys. Rev. D* **100** no. 10, (2019) 104036, [arXiv:1903.04467](https://arxiv.org/abs/1903.04467) [gr-qc].
- [4] C. V. Vishveshvara, “Stability of the schwarzschild metric,” *Phys. Rev.* **D1** (1970) 2870–2879.
- [5] S. Chandrasekhar, *The mathematical theory of black holes*. 1985.
- [6] S. Detweiler, “Black holes and gravitational waves. III - The resonant frequencies of rotating holes,” *Astrophys. J.* **239** (July, 1980) 292–295.
- [7] O. Dreyer, B. J. Kelly, B. Krishnan, L. S. Finn, D. Garrison, and R. Lopez-Aleman, “Black hole spectroscopy: Testing general relativity through gravitational wave observations,” *Class. Quant. Grav.* **21** (2004) 787–804, [arXiv:gr-qc/0309007](https://arxiv.org/abs/gr-qc/0309007) [gr-qc].
- [8] E. Berti, V. Cardoso, and C. M. Will, “On gravitational-wave spectroscopy of massive black holes with the space interferometer LISA,” *Phys. Rev.* **D73** (2006) 064030, [arXiv:gr-qc/0512160](https://arxiv.org/abs/gr-qc/0512160) [gr-qc].
- [9] K. D. Kokkotas and B. G. Schmidt, “Quasinormal modes of stars and black holes,” *Living Rev. Rel.* **2** (1999) 2, [arXiv:gr-qc/9909058](https://arxiv.org/abs/gr-qc/9909058) [gr-qc].
- [10] E. Berti, V. Cardoso, and A. O. Starinets, “Quasinormal modes of black holes and black branes,” *Class. Quantum Grav.* **26** (2009) 163001, [arXiv:0905.2975](https://arxiv.org/abs/0905.2975) [gr-qc].
- [11] **The LIGO/Virgo Scientific Collaboration** Collaboration, B. P. Abbott *et al.*, “Observation of Gravitational Waves from a Binary Black Hole Merger,” *Phys. Rev. Lett.* **116** no. 6, (2016) 061102, [arXiv:1602.03837](https://arxiv.org/abs/1602.03837) [gr-qc].
- [12] E. Berti *et al.*, “Testing General Relativity with Present and Future Astrophysical Observations,” *Class. Quant. Grav.* **32** (2015) 243001, [arXiv:1501.07274](https://arxiv.org/abs/1501.07274) [gr-qc].
- [13] L. Barack *et al.*, “Black holes, gravitational waves and fundamental physics: a roadmap,” [arXiv:1806.05195](https://arxiv.org/abs/1806.05195)

- [gr-qc].
- [14] E. Berti, K. Yagi, H. Yang, and N. Yunes, “Extreme Gravity Tests with Gravitational Waves from Compact Binary Coalescences: (II) Ringdown,” *Gen. Rel. Grav.* **50** no. 5, (2018) 49, [arXiv:1801.03587 \[gr-qc\]](#).
- [15] B. S. Sathyaprakash *et al.*, “Extreme Gravity and Fundamental Physics,” [arXiv:1903.09221 \[astro-ph.HE\]](#).
- [16] S. Hawking, “Particle Creation by Black Holes,” *Commun. Math. Phys.* **43** (1975) 199–220. [Erratum: *Commun. Math. Phys.* **46**, 206 (1976)].
- [17] V. Cardoso and P. Pani, “Testing the nature of dark compact objects: a status report,” *Living Rev. Rel.* **22** no. 1, (2019) 4, [arXiv:1904.05363 \[gr-qc\]](#).
- [18] V. Cardoso, L. C. B. Crispino, C. F. B. Macedo, H. Okawa, and P. Pani, “Light rings as observational evidence for event horizons: long-lived modes, ergoregions and nonlinear instabilities of ultracompact objects,” *Phys. Rev.* **D90** no. 4, (2014) 044069, [arXiv:1406.5510 \[gr-qc\]](#).
- [19] P. V. Cunha and C. A. Herdeiro, “Stationary black holes and light rings,” *Phys. Rev. Lett.* **124** no. 18, (2020) 181101, [arXiv:2003.06445 \[gr-qc\]](#).
- [20] S. Hawking, “Breakdown of Predictability in Gravitational Collapse,” *Phys. Rev. D* **14** (1976) 2460–2473.
- [21] O. Lunin and S. D. Mathur, “AdS / CFT duality and the black hole information paradox,” *Nucl. Phys. B* **623** (2002) 342–394, [arXiv:hep-th/0109154](#).
- [22] O. Lunin and S. D. Mathur, “Statistical interpretation of Bekenstein entropy for systems with a stretched horizon,” *Phys. Rev. Lett.* **88** (2002) 211303, [arXiv:hep-th/0202072 \[hep-th\]](#).
- [23] S. D. Mathur, “The Fuzzball proposal for black holes: An Elementary review,” *Fortsch. Phys.* **53** (2005) 793–827, [arXiv:hep-th/0502050 \[hep-th\]](#).
- [24] R. C. Myers, “Pure states don’t wear black,” *Gen. Rel. Grav.* **29** (1997) 1217–1222, [arXiv:gr-qc/9705065 \[gr-qc\]](#).
- [25] I. Bena and N. P. Warner, “Black holes, black rings and their microstates,” *Lect. Notes Phys.* **755** (2008) 1–92, [arXiv:hep-th/0701216 \[hep-th\]](#).
- [26] V. Balasubramanian, J. de Boer, S. El-Showk, and I. Messamah, “Black Holes as Effective Geometries,” *Class. Quant. Grav.* **25** (2008) 214004, [arXiv:0811.0263 \[hep-th\]](#).
- [27] I. Bena and N. P. Warner, “Resolving the Structure of Black Holes: Philosophizing with a Hammer,” [arXiv:1311.4538 \[hep-th\]](#).
- [28] L. Buoninfante and A. Mazumdar, “Nonlocal star as a blackhole mimicker,” *Phys. Rev. D* **100** no. 2, (2019) 024031, [arXiv:1903.01542 \[gr-qc\]](#).
- [29] P. Nicolini, A. Smailagic, and E. Spallucci, “Noncommutative geometry inspired Schwarzschild black hole,” *Phys. Lett. B* **632** (2006) 547–551, [arXiv:gr-qc/0510112](#).
- [30] A. S. Koshelev and A. Mazumdar, “Do massive compact objects without event horizon exist in infinite derivative gravity?,” *Phys. Rev.* **D96** no. 8, (2017) 084069, [arXiv:1707.00273 \[gr-qc\]](#).
- [31] L. Buoninfante, A. S. Koshelev, G. Lambiase, J. Marto, and A. Mazumdar, “Conformally-flat, non-singular static metric in infinite derivative gravity,” *JCAP* **1806** no. 06, (2018) 014, [arXiv:1804.08195 \[gr-qc\]](#).
- [32] L. Buoninfante, A. S. Cornell, G. Harmsen, A. S. Koshelev, G. Lambiase, J. Marto, and A. Mazumdar, “Towards nonsingular rotating compact object in ghost-free infinite derivative gravity,” *Phys. Rev. D* **98** no. 8, (2018) 084041, [arXiv:1807.08896 \[gr-qc\]](#).
- [33] T. Biswas, E. Gerwick, T. Koivisto, and A. Mazumdar, “Towards singularity and ghost free theories of gravity,” *Phys. Rev. Lett.* **108** (2012) 031101, [arXiv:1110.5249 \[gr-qc\]](#).
- [34] V. P. Frolov, “Mass-gap for black hole formation in higher derivative and ghost free gravity,” *Phys. Rev. Lett.* **115** no. 5, (2015) 051102, [arXiv:1505.00492 \[hep-th\]](#).
- [35] **LIGO Scientific, Virgo Collaboration**, R. Abbott *et al.*, “GW190814: Gravitational Waves from the Coalescence of a 23 Solar Mass Black Hole with a 2.6 Solar Mass Compact Object,” *Astrophys. J.* **896** no. 2, (2020) L44, [arXiv:2006.12611 \[astro-ph.HE\]](#).
- [36] T. Damour, “Surface Effects in Black-Hole Physics,” in *Marcel Grossmann Meeting: General Relativity*, p. 587. Jan., 1982.
- [37] K. S. Thorne, R. Price, and D. Macdonald, eds., *BLACK HOLES: THE MEMBRANE PARADIGM*. 1986.
- [38] V. Cardoso, E. Franzin, and P. Pani, “Is the gravitational-wave ringdown a probe of the event horizon?,” *Phys. Rev. Lett.* **116** no. 17, (2016) 171101, [arXiv:1602.07309 \[gr-qc\]](#).
- [39] V. Cardoso, S. Hopper, C. F. B. Macedo, C. Palenzuela, and P. Pani, “Gravitational-wave signatures of exotic compact objects and of quantum corrections at the horizon scale,” *Phys. Rev.* **D94** no. 8, (2016) 084031, [arXiv:1608.08637 \[gr-qc\]](#).
- [40] V. Cardoso and P. Pani, “Tests for the existence of black holes through gravitational wave echoes,” *Nat. Astron.* **1** no. 9, (2017) 586–591, [arXiv:1709.01525 \[gr-qc\]](#).
- [41] Z. Mark, A. Zimmerman, S. M. Du, and Y. Chen, “A recipe for echoes from exotic compact objects,” *Phys. Rev.* **D96** no. 8, (2017) 084002, [arXiv:1706.06155 \[gr-qc\]](#).
- [42] E. Maggio, P. Pani, and V. Ferrari, “Exotic Compact Objects and How to Quench their Ergoregion Instability,” *Phys. Rev.* **D96** no. 10, (2017) 104047, [arXiv:1703.03696 \[gr-qc\]](#).
- [43] J. Abedi, H. Dykaar, and N. Afshordi, “Echoes from the Abyss: Tentative evidence for Planck-scale structure at black hole horizons,” *Phys. Rev.* **D96** no. 8, (2017) 082004, [arXiv:1612.00266 \[gr-qc\]](#).
- [44] R. S. Conklin, B. Holdom, and J. Ren, “Gravitational wave echoes through new windows,” *Phys. Rev.* **D98** no. 4, (2018) 044021, [arXiv:1712.06517 \[gr-qc\]](#).
- [45] N. Oshita and N. Afshordi, “Probing microstructure of black hole spacetimes with gravitational wave echoes,” *Phys. Rev.* **D99** no. 4, (2019) 044002, [arXiv:1807.10287 \[gr-qc\]](#).
- [46] Q. Wang, N. Oshita, and N. Afshordi, “Echoes from Quantum Black Holes,” *Phys. Rev. D* **101** no. 2, (2020) 024031, [arXiv:1905.00446 \[gr-qc\]](#).
- [47] V. Cardoso, V. F. Foit, and M. Kleban, “Gravitational wave echoes from black hole area quantization,” *JCAP* **08** (2019) 006, [arXiv:1902.10164 \[hep-th\]](#).
- [48] A. Coates, S. H. Völkel, and K. D. Kokkotas, “Spectral

- Lines of Quantized, Spinning Black Holes and their Astrophysical Relevance,” *Phys. Rev. Lett.* **123** no. 17, (2019) 171104, [arXiv:1909.01254 \[gr-qc\]](#).
- [49] L. Buoninfante, “Echoes from corpuscular black holes,” [arXiv:2005.08426 \[gr-qc\]](#).
- [50] V. Ferrari and K. D. Kokkotas, “Scattering of particles by neutron stars: Time evolutions for axial perturbations,” *Phys. Rev.* **D62** (2000) 107504, [arXiv:gr-qc/0008057 \[gr-qc\]](#).
- [51] P. Pani and V. Ferrari, “On gravitational-wave echoes from neutron-star binary coalescences,” *Class. Quant. Grav.* **35** no. 15, (2018) 15LT01, [arXiv:1804.01444 \[gr-qc\]](#).
- [52] B. Holdom and J. Ren, “Not quite a black hole,” *Phys. Rev.* **D95** no. 8, (2017) 084034, [arXiv:1612.04889 \[gr-qc\]](#).
- [53] L. Buoninfante, A. Mazumdar, and J. Peng, “Nonlocality amplifies echoes,” *Phys. Rev. D* **100** no. 10, (2019) 104059, [arXiv:1906.03624 \[gr-qc\]](#).
- [54] A. Delhom, C. F. Macedo, G. J. Olmo, and L. C. Crispino, “Absorption by black hole remnants in metric-affine gravity,” *Phys. Rev. D* **100** no. 2, (2019) 024016, [arXiv:1906.06411 \[gr-qc\]](#).
- [55] H. Nakano, N. Sago, H. Tagoshi, and T. Tanaka, “Black hole ringdown echoes and howls,” *PTEP* **2017** no. 7, (2017) 071E01, [arXiv:1704.07175 \[gr-qc\]](#).
- [56] P. Bueno, P. A. Cano, F. Goelen, T. Hertog, and B. Vercknocke, “Echoes of Kerr-like wormholes,” *Phys. Rev.* **D97** no. 2, (2018) 024040, [arXiv:1711.00391 \[gr-qc\]](#).
- [57] Y.-T. Wang, Z.-P. Li, J. Zhang, S.-Y. Zhou, and Y.-S. Piao, “Are gravitational wave ringdown echoes always equal-interval?,” *Eur. Phys. J.* **C78** no. 6, (2018) 482, [arXiv:1802.02003 \[gr-qc\]](#).
- [58] M. R. Correia and V. Cardoso, “Characterization of echoes: A Dyson-series representation of individual pulses,” *Phys. Rev.* **D97** no. 8, (2018) 084030, [arXiv:1802.07735 \[gr-qc\]](#).
- [59] Q. Wang and N. Afshordi, “Black hole echology: The observer’s manual,” *Phys. Rev.* **D97** no. 12, (2018) 124044, [arXiv:1803.02845 \[gr-qc\]](#).
- [60] N. Uchikata, H. Nakano, T. Narikawa, N. Sago, H. Tagoshi, and T. Tanaka, “Searching for black hole echoes from the LIGO-Virgo Catalog GWTC-1,” *Phys. Rev. D* **100** no. 6, (2019) 062006, [arXiv:1906.00838 \[gr-qc\]](#).
- [61] A. Testa and P. Pani, “Analytical template for gravitational-wave echoes: signal characterization and prospects of detection with current and future interferometers,” *Phys. Rev.* **D98** no. 4, (2018) 044018, [arXiv:1806.04253 \[gr-qc\]](#).
- [62] E. Maggio, A. Testa, S. Bhagwat, and P. Pani, “Analytical model for gravitational-wave echoes from spinning remnants,” *Phys. Rev. D* **100** no. 6, (2019) 064056, [arXiv:1907.03091 \[gr-qc\]](#).
- [63] G. Ashton, O. Birnholtz, M. Cabero, C. Capano, T. Dent, B. Krishnan, G. D. Meadors, A. B. Nielsen, A. Nitz, and J. Westerweck, “Comments on: ”Echoes from the abyss: Evidence for Planck-scale structure at black hole horizons”,” [arXiv:1612.05625 \[gr-qc\]](#).
- [64] J. Abedi, H. Dykaar, and N. Afshordi, “Echoes from the Abyss: The Holiday Edition!,” [arXiv:1701.03485 \[gr-qc\]](#).
- [65] J. Westerweck, A. Nielsen, O. Fischer-Birnholtz, M. Cabero, C. Capano, T. Dent, B. Krishnan, G. Meadors, and A. H. Nitz, “Low significance of evidence for black hole echoes in gravitational wave data,” *Phys. Rev.* **D97** no. 12, (2018) 124037, [arXiv:1712.09966 \[gr-qc\]](#).
- [66] J. Abedi, H. Dykaar, and N. Afshordi, “Comment on: ”Low significance of evidence for black hole echoes in gravitational wave data”,,” [arXiv:1803.08565 \[gr-qc\]](#).
- [67] R. S. Conklin and B. Holdom, “Gravitational Wave ”Echo” Spectra,” [arXiv:1905.09370 \[gr-qc\]](#).
- [68] K. W. Tsang, A. Ghosh, A. Samajdar, K. Chatziioannou, S. Mastrogiovanni, M. Agathos, and C. Van Den Broeck, “A morphology-independent search for gravitational wave echoes in data from the first and second observing runs of Advanced LIGO and Advanced Virgo,” *Phys. Rev. D* **101** no. 6, (2020) 064012, [arXiv:1906.11168 \[gr-qc\]](#).
- [69] J. Abedi, N. Afshordi, N. Oshita, and Q. Wang, “Quantum Black Holes in the Sky,” *Universe* **6** no. 3, (2020) 43, [arXiv:2001.09553 \[gr-qc\]](#).
- [70] B. Guo, S. Hampton, and S. D. Mathur, “Can we observe fuzzballs or firewalls?,” *JHEP* **07** (2018) 162, [arXiv:1711.01617 \[hep-th\]](#).
- [71] R. Price and K. Thorne, “Membrane Viewpoint on Black Holes: Properties and Evolution of the Stretched Horizon,” *Phys. Rev. D* **33** (1986) 915–941.
- [72] G. Darmois, *Les équations de la gravitation einsteinienne*. Gauthier-Villars, 1927. <http://eudml.org/doc/192556>.
- [73] W. Israel, “Singular hypersurfaces and thin shells in general relativity,” *Nuovo Cim.* **B44S10** (1966) 1. [Nuovo Cim.B44,1(1966)].
- [74] M. Visser, *Lorentzian wormholes: From Einstein to Hawking*. AIP, Woodbury, USA, 1996.
- [75] T. Jacobson, A. Mohd, and S. Sarkar, “Membrane paradigm for Einstein-Gauss-Bonnet gravity,” *Phys. Rev. D* **95** no. 6, (2017) 064036, [arXiv:1107.1260 \[gr-qc\]](#).
- [76] H. A. Buchdahl, “General Relativistic Fluid Spheres,” *Phys. Rev.* **116** (1959) 1027.
- [77] N. Oshita, Q. Wang, and N. Afshordi, “On Reflectivity of Quantum Black Hole Horizons,” *JCAP* **04** (2020) 016, [arXiv:1905.00464 \[hep-th\]](#).
- [78] T. Regge and J. A. Wheeler, “Stability of a Schwarzschild singularity,” *Phys. Rev.* **108** (1957) 1063–1069.
- [79] F. J. Zerilli, “Effective potential for even parity Regge-Wheeler gravitational perturbation equations,” *Phys. Rev. Lett.* **24** (1970) 737–738.
- [80] F. Zerilli, “Gravitational field of a particle falling in a schwarzschild geometry analyzed in tensor harmonics,” *Phys. Rev.* **D2** (1970) 2141–2160.
- [81] E. Maggio, V. Cardoso, S. R. Dolan, and P. Pani, “Ergoregion instability of exotic compact objects: electromagnetic and gravitational perturbations and the role of absorption,” *Phys. Rev.* **D99** no. 6, (2019) 064007, [arXiv:1807.08840 \[gr-qc\]](#).
- [82] R. Brito, V. Cardoso, and P. Pani, “Superradiance,” *Lect. Notes Phys.* **906** (2015) pp.1–237, [arXiv:1501.06570 \[gr-qc\]](#).
- [83] M. Visser and D. L. Wiltshire, “Stable gravastars: An Alternative to black holes?,” *Class. Quant. Grav.* **21** (2004) 1135–1152, [arXiv:gr-qc/0310107 \[gr-qc\]](#).

- [84] P. Pani, E. Berti, V. Cardoso, Y. Chen, and R. Norte, “Gravitational-wave signatures of the absence of an event horizon. II. Extreme mass ratio inspirals in the spacetime of a thin-shell gravastar,” *Phys. Rev.* **D81** (2010) 084011, [arXiv:1001.3031 \[gr-qc\]](#).
- [85] P. Pani, “Advanced Methods in Black-Hole Perturbation Theory,” *Int. J. Mod. Phys.* **A28** (2013) 1340018, [arXiv:1305.6759 \[gr-qc\]](#).
- [86] E. Leaver, “An Analytic representation for the quasi normal modes of Kerr black holes,” *Proc. Roy. Soc. Lond. A* **A402** (1985) 285–298.
- [87] M. Leins, H. Nollert, and M. Soffel, “Nonradial oscillations of neutron stars: A New branch of strongly damped normal modes,” *Phys. Rev. D* **48** (1993) 3467–3472.
- [88] O. Benhar, E. Berti, and V. Ferrari, “The Imprint of the equation of state on the axial w modes of oscillating neutron stars,” *ICTP Lect. Notes Ser.* **3** (2001) 35–46, [arXiv:gr-qc/9901037](#).
- [89] P. Pani, E. Berti, V. Cardoso, Y. Chen, and R. Norte, “Gravitational wave signatures of the absence of an event horizon. I. Nonradial oscillations of a thin-shell gravastar,” *Phys. Rev.* **D80** (2009) 124047, [arXiv:0909.0287 \[gr-qc\]](#).
- [90] S. Chandrasekhar and S. L. Detweiler, “The quasi-normal modes of the Schwarzschild black hole,” *Proc. Roy. Soc. Lond. A* **A344** (1975) 441–452.
- [91] M. Giesler, M. Isi, M. A. Scheel, and S. Teukolsky, “Black Hole Ringdown: The Importance of Overtones,” *Phys. Rev. X* **9** no. 4, (2019) 041060, [arXiv:1903.08284 \[gr-qc\]](#).
- [92] M. Isi, M. Giesler, W. M. Farr, M. A. Scheel, and S. A. Teukolsky, “Testing the no-hair theorem with GW150914,” *Phys. Rev. Lett.* **123** no. 11, (2019) 111102, [arXiv:1905.00869 \[gr-qc\]](#).
- [93] E. Berti, J. Cardoso, V. Cardoso, and M. Cavaglia, “Matched-filtering and parameter estimation of ringdown waveforms,” *Phys. Rev.* **D76** (2007) 104044, [arXiv:0707.1202 \[gr-qc\]](#).
- [94] V. Baibhav, E. Berti, V. Cardoso, and G. Khanna, “Black Hole Spectroscopy: Systematic Errors and Ringdown Energy Estimates,” *Phys. Rev.* **D97** no. 4, (2018) 044048, [arXiv:1710.02156 \[gr-qc\]](#).
- [95] S. Bhagwat, X. J. Forteza, P. Pani, and V. Ferrari, “Ringdown overtones, black hole spectroscopy, and no-hair theorem tests,” *Phys. Rev. D* **101** no. 4, (2020) 044033, [arXiv:1910.08708 \[gr-qc\]](#).
- [96] I. Ota and C. Chirenti, “Overtones or higher harmonics? Prospects for testing the no-hair theorem with gravitational wave detections,” *Phys. Rev. D* **101** no. 10, (2020) 104005, [arXiv:1911.00440 \[gr-qc\]](#).
- [97] X. J. Forteza, S. Bhagwat, P. Pani, and V. Ferrari, “On the spectroscopy of binary black hole ringdown using overtones and angular modes,” [arXiv:2005.03260 \[gr-qc\]](#).
- [98] H.-P. Nollert, “About the significance of quasinormal modes of black holes,” *Phys. Rev. D* **53** (1996) 4397–4402, [arXiv:gr-qc/9602032](#).
- [99] P. Leung, Y. Liu, W. Suen, C. Tam, and K. Young, “Perturbative approach to the quasinormal modes of dirty black holes,” *Phys. Rev. D* **59** (1999) 044034, [arXiv:gr-qc/9903032](#).
- [100] E. Barausse, V. Cardoso, and P. Pani, “Can environmental effects spoil precision gravitational-wave astrophysics?,” *Phys. Rev.* **D89** no. 10, (2014) 104059, [arXiv:1404.7149 \[gr-qc\]](#).
- [101] J. L. Jaramillo, R. Panosso Macedo, and L. Al Sheikh, “Pseudospectrum and black hole quasi-normal mode (in)stability,” [arXiv:2004.06434 \[gr-qc\]](#).
- [102] S. Hild *et al.*, “Sensitivity Studies for Third-Generation Gravitational Wave Observatories,” *Class. Quant. Grav.* **28** (2011) 094013, [arXiv:1012.0908 \[gr-qc\]](#).
- [103] H. Audley, S. Babak, J. Baker, E. Barausse, P. Bender, E. Berti, P. Binetruy, M. Born, D. Bortoluzzi, J. Camp, C. Caprini, V. Cardoso, M. Colpi, J. Conklin, N. Cornish, C. Cutler, *et al.*, “Laser Interferometer Space Antenna,” *ArXiv e-prints* (Feb., 2017) , [arXiv:1702.00786 \[astro-ph.IM\]](#).
- [104] V. Baibhav *et al.*, “Probing the Nature of Black Holes: Deep in the mHz Gravitational-Wave Sky,” [arXiv:1908.11390 \[astro-ph.HE\]](#).
- [105] T. Damour and S. N. Solodukhin, “Wormholes as black hole foils,” *Phys. Rev.* **D76** (2007) 024016, [arXiv:0704.2667 \[gr-qc\]](#).
- [106] P. O. Mazur and E. Mottola, “Gravitational vacuum condensate stars,” *Proc. Nat. Acad. Sci.* **101** (2004) 9545–9550, [arXiv:gr-qc/0407075 \[gr-qc\]](#).
- [107] C. B. M. H. Chirenti and L. Rezzolla, “How to tell a gravastar from a black hole,” *Class. Quant. Grav.* **24** (2007) 4191–4206, [arXiv:0706.1513 \[gr-qc\]](#).
- [108] E. G. Gimon and P. Horava, “Astrophysical violations of the Kerr bound as a possible signature of string theory,” *Phys. Lett.* **B672** (2009) 299–302, [arXiv:0706.2873 \[hep-th\]](#).
- [109] C. O. Lousto and B. F. Whiting, “Reconstruction of black hole metric perturbations from Weyl curvature,” *Phys. Rev. D* **66** (2002) 024026, [arXiv:gr-qc/0203061](#).
- [110] B. Whiting and L. Price, “Metric reconstruction from Weyl scalars,” *Class. Quant. Grav.* **22** (2005) S589–S604.
- [111] G. Raposo, P. Pani, and R. Emparan, “Exotic compact objects with soft hair,” *Phys. Rev.* **D99** no. 10, (2019) 104050, [arXiv:1812.07615 \[gr-qc\]](#).
- [112] V. Cardoso, P. Pani, M. Cadoni, and M. Cavaglia, “Ergoregion instability of ultracompact astrophysical objects,” *Phys. Rev.* **D77** (2008) 124044, [arXiv:0709.0532 \[gr-qc\]](#).
- [113] V. Cardoso, P. Pani, M. Cadoni, and M. Cavaglia, “Instability of hyper-compact Kerr-like objects,” *Class. Quant. Grav.* **25** (2008) 195010, [arXiv:0808.1615 \[gr-qc\]](#).
- [114] P. Pani, E. Barausse, E. Berti, and V. Cardoso, “Gravitational instabilities of superspinars,” *Phys. Rev.* **D82** (2010) 044009, [arXiv:1006.1863 \[gr-qc\]](#).
- [115] Y. Kojima, “Equations governing the nonradial oscillations of a slowly rotating relativistic star,” *Phys. Rev. D* **46** (1992) 4289–4303.
- [116] N. Uchikata, S. Yoshida, and P. Pani, “Tidal deformability and I-Love-Q relations for gravastars with polytropic thin shells,” *Phys. Rev.* **D94** no. 6, (2016) 064015, [arXiv:1607.03593 \[gr-qc\]](#).